

# Investigation of residual stresses of hybrid normal and high strength steel (HNHSS) welded box sections

Lan Kang<sup>\*1,2</sup>, Yuqi Wang<sup>1,2</sup>, Xinpei Liu<sup>3</sup> and Brian Uy<sup>3</sup>

<sup>1</sup> School of Civil Engineering and Transportation, South China University of Technology, Guangzhou, Guangdong Province, 510641, People's Republic of China

<sup>2</sup> State Key Laboratory of Subtropical Building Science, South China University of Technology, Guangzhou, Guangdong Province, 510641, People's Republic of China

<sup>3</sup> School of Civil Engineering, Faculty of Engineering & Information Technologies, The University of Sydney, NSW 2006, Australia

(Received May 28, 2019, Revised September 24, 2019, Accepted October 2, 2019)

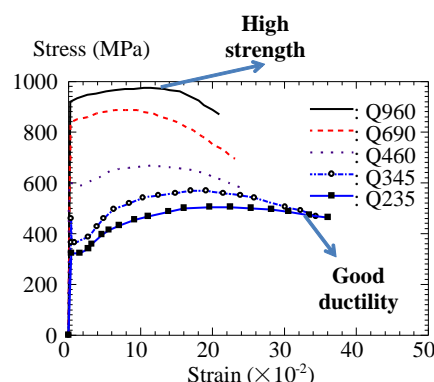
**Abstract.** In order to obtain high bearing capacity and good ductility simultaneously, a structural column with hybrid normal and high strength steel (HNHSS) welded box section has been developed. Residual stress is an important factor that can influence the behaviour of a structural member in steel structures. Accordingly, the magnitudes and distributions of residual stresses in HNHSS welded box sections were investigated experimentally using the sectioning method. In this study, the following four box sections were tested: one normal strength steel (NSS) section, one high strength steel (HSS) section, and two HNHSS sections. Based on the experimental data from previous studies and the test results of this study, the effects of the width-to-thickness ratio of plate, yield strength of plate, and the plate thickness of the residual stresses of welded box sections were investigated in detail. A unified residual stress model for NSS, HSS and HNHSS welded box sections was proposed, and the corresponding simplified prediction equations for the maximum tensile residual stress ratio ( $\sigma_r/f_y$ ) and average compressive residual stress ratio ( $\sigma_c/f_y$ ) in the model were quantitatively established. The predicted magnitudes and distributions of residual stresses for four tested sections in this study by using the proposed residual stress model were compared with the experimental results, and the feasibility of this proposed model was shown to be in good agreement.

**Keywords:** residual stress; hybrid box section; sectioning method; high strength steel

## 1. Introduction

Although high strength steel (HSS) structures have a significant advantage in improving the vertical bearing capacity of structures, the application of HSS in seismic structures is limited owing to its relatively poor ductility compared with that of normal strength steel (NSS). It can be observed that the length of the yield plateau for HSS is shortened (or even disappears) compared with that for NSS (Qiang *et al.* 2016, Choi and Kwon 2018, Feng and Qian 2018, Kang *et al.* 2018a, b, Cai and Young 2019), as illustrated in Fig. 1, in which Q235 and Q345 are normal strength steel, and Q460, Q690, Q960 are high strength steel. This shortcoming limits the application of HSS in seismic areas (Lian *et al.* 2015, Javidan *et al.* 2016, 2018, Farahi and Erfani 2017, Fang *et al.* 2018, Saliba *et al.* 2018, Chen and Shi 2019). Hence, overcoming this shortcoming of HSS is very important. Steel columns with NSS or HSS sections as shown in Fig. 2 have been popularly employed in steel structures. The skeleton curves of steel columns with different sections under lateral cyclic loading are shown in Fig. 3. It is observed that the lateral load bearing capacity of HSS columns is higher than that of NSS

columns, whereas their ductility is significantly less than that of NSS columns. To obtain high bearing capacity and good ductility simultaneously, a structural column with a new type of hybrid normal and high strength steel (HNHSS) welded box section (denoted as Sections B-345-10-690-10 and B-345-20-690-10 in Fig. 2) was proposed. In the hybrid section, the flange plates perpendicular to the direction of cyclic loading were fabricated using NSS Q345 steel plates in order to improve the ductility of structural member, while the web plates parallel to the direction of cyclic loading



Normal strength steel (NSS): Q235, Q345;  
High strength steel (HSS): Q460, Q690, Q960

Fig. 1 Stress-strain curves of NSS and HSS

\*Corresponding author, Ph.D., Associated Professor,  
E-mail: [ctlkang@scut.edu.cn](mailto:ctlkang@scut.edu.cn)

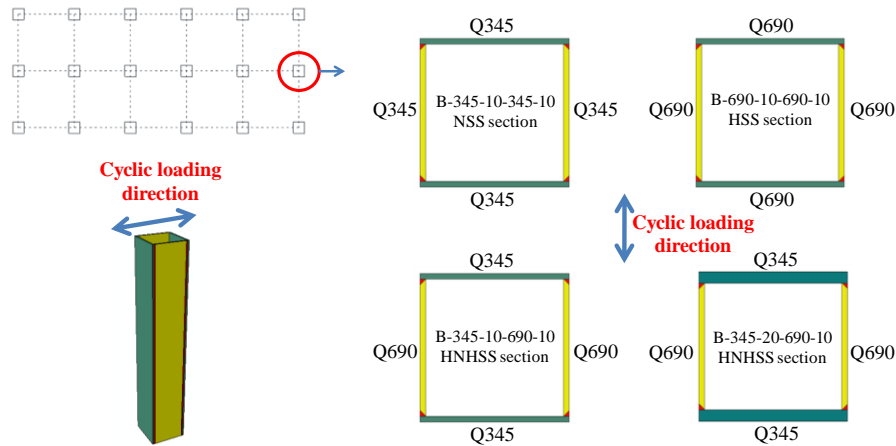


Fig. 2 Mechanism of HNHSS sections

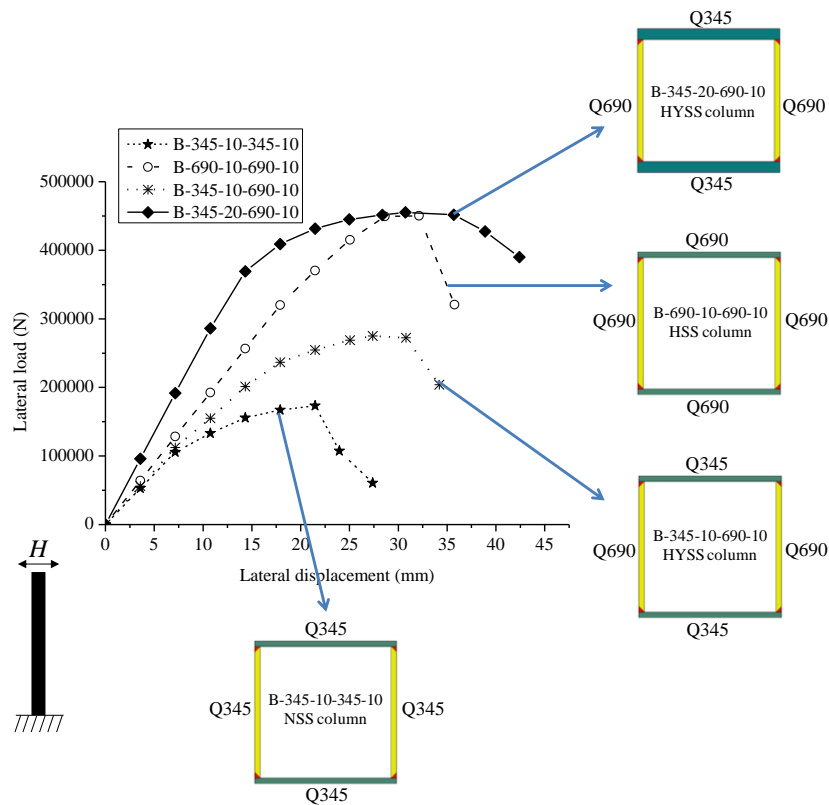


Fig. 3 Skeleton curves of steel columns with four different sections

were fabricated using HSS Q690 plates to obtain high axial and lateral load bearing capacities. A total of four sections as listed in Table 1 were analysed to preliminary study the difference of seismic performance of steel columns with NSS, HSS and HNHSS sections. The height of four steel columns is 1.20 m. The material properties are listed in Table 2. It can be clearly observed from the skeleton curves obtained from the finite element analyses (as shown in Fig. 3) that the ductility of the columns with HNHSS sections is significantly improved compared to that of HSS columns, and the lateral load bearing capacity of the columns with HNHSS sections is much larger than that of the columns with NSS sections. Therefore, a column with HNHSS

section can exhibit better seismic performance compared with the one with HSS or NSS section. Certainly, as the direction of the earthquake action is random, and designers may not ensure one component plate to be always perpendicular to the seismic loading direction. In order to overcome this issue, a chessboard layout as shown in Fig. 4 can be applied to ensure that the whole structure has good seismic performance in all directions. However, the residual stresses of HNHSS box sections are different from those of NSS and HSS sections due to the effect of welds. The residual stress models for NSS and HSS sections are unsuitable for HNHSS sections. Because residual stress has significant influences on the behaviour of steel columns

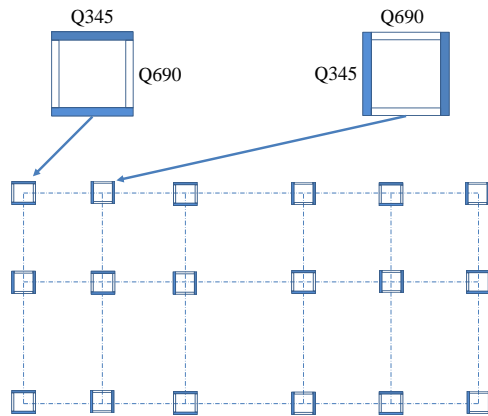


Fig. 4 Chessboard layout

with HNHSS box sections, it is crucial to establish a simplified model for estimating the distributions and magnitudes of residual stresses in HNHSS box sections. For NSS sections, many investigations considering a residual stress model have been undertaken in the past (Nagaraja Rao and Tall 1961, Estuar and Tall 1963, Tebedge *et al.* 1973, Klotz *et al.* 2002, Besevic 2012, Hwang *et al.* 2015, Zhang *et al.* 2016, Chen *et al.* 2018, Wang *et al.* 2018). A total of nine stub column tests for the measurement of residual stresses were carried out by Gardner *et al.* (2016)

on NSS I-shape welded members. Residual stress distribution measurement tests were conducted by Yuan *et al.* (2014) for ten I-sections, four square hollow sections and four rectangular hollow sections assembled by means of shielded metal arc welding (SMAW). Among these investigations, the sectioning method is the most common method for measuring residual stress (Gou *et al.* 2014, Zhang *et al.* 2016, 2019, Taheri-Behrooz *et al.* 2018, An *et al.* 2019, Wang *et al.* 2019). Based on these previous experimental results, different residual stress models for various sectional types were well established and further employed in Eurocode 3 (2005), ANSI/AISC360-10 (2010) and Chinese code GB50017-2017 (2017).

In the case of HSS sections, some residual stress tests have been performed, and some reliable results have been obtained for the residual stresses of HSS welded sections. Nie *et al.* (2018) gauged the residual stresses in eight box sections fabricated from Q460GJ steel with different width-to-thickness ratios using the sectioning method. Somodi and Kövesdi (2018) gauged the residual stresses in 21 box sections fabricated from S235-S960 steels in order to study the influence of steel grade on the residual stresses of welded sections. They also measured the residual stresses in 13 cold-formed HSS hollow section columns (Somodi and Kovesdi 2017). Cao *et al.* (2018) performed experiments for measuring the residual stresses of HSS welded box sections, in which the yield strength of HSS was 800 MPa. Khan *et*

Table 1 Design and measured specimen sectional dimensions

Section label	Design sectional height $H_{des}$ (mm)	Design sectional width $B_{des}$ (mm)	Design flange thickness $t_{f,des}$ (mm)	Design web thickness $t_{w,des}$ (mm)	$b_{f,des}/t_{f,des}$	$h_{0,des}/t_{w,des}$
B-345-10-345-10	260	260	10	10	24	24
B-690-10-690-10	260	260	10	10	24	24
B-345-10-690-10	260	260	10	10	24	24
B-345-20-690-10	260	260	20	10	12	22
Section label	Measured sectional height $H$ (mm)	Measured sectional width $B$ (mm)	Measured flange thickness $t_f$ (mm)	Measured web thickness $t_w$ (mm)	$b_f/t_f$	$h_0/t_w$
B-345-10-345-10	257.0	259.0	10.18	10.10	23.46	23.43
B-690-10-690-10	259.5	261.0	10.60	10.59	22.63	22.50
B-345-10-690-10	260.5	259.0	10.17	10.60	23.38	22.66
B-345-20-690-10	258.5	262.5	19.98	10.63	12.07	20.56

\*Notes: In section label, "B" means box section, the first numeral is the steel grade of flange plate, the second numeral is the design thickness of flange plate, the third numeral is the steel grade of web plate and the forth numeral is the design thickness of web plate. For example, B-345-20-690-10 means such a specimen, in which the flange plates are Q345 steel plates with the design thickness of 20 mm, and the web plates are Q690 steel plates with the design thickness of 10 mm.  $h_0/t_w$  and  $b_f/t_f$  represent the width-to-thickness ratios of web and flange, respectively

Table 2 Material properties

Steel grade	Design thickness of steel plates $t_{des}$ (mm)	Elastic modulus $E$ (GPa)	Yield strength $f_y$ (MPa)	Ultimate strength $f_u$ (MPa)	Poisson ratio $\nu$
Q345	10	211.80	393.04	544.22	0.28
Q345	20	213.57	379.28	527.42	0.28
Q690	10	218.09	757.84	803.20	0.29

\*Notes:  $E$  is the Young's modulus,  $f_y$  is the yield strength,  $f_u$  is the ultimate strength, and  $\nu$  is the Poisson ratio

*al.* (2016) investigated the distributions of residual stresses in square welded sections with single and multiple weld passes. The sections were fabricated from HSS plates with yield strength of 690 MPa. The residual stresses of two built-up box T-joints fabricated from HSS plates with a yield stress of 690 MPa were measured by Jiang *et al.* (2015). Residual stress measurement tests were conducted by Li *et al.* (2015) on welded Q690 HSS box- and H-sections. Ban *et al.* (2013) experimentally measured the residual stresses of welded sections including box and I-shape sections by using the sectioning method. The maximum yield strength was determined as 960 MPa, and some sensitive factors such as the steel plate thickness, web or flange width-to-thickness ratios, welding type, and the interaction between the flange and web plates, were also taken into consideration. Wang *et al.* (2012) gauged the residual stresses of box- and H-shaped sections fabricated from HSS steel plates with a yield strength of 460 MPa by applying both the hole drilling method and sectioning method. These investigations provided several important findings. However, there were too many different residual stress models proposed for the box sections fabricated using different grades of steels, which are not convenient for the application of engineers and researchers. Therefore, it is necessary to establish a unified model for estimating the residual stress of box sections fabricated using steels of different strengths.

In this paper, an experimental investigation is described to discuss the residual stress magnitudes and distributions of four welded box sections: one fabricated from Q345 steel, one fabricated from Q690 steel, and two fabricated from Q345 and Q690 steels. The measured values of the longitudinal residual stresses were acquired using the sectioning method. The effects of the steel grade, width-to-

thickness ratio, plate thickness, and the interactions between four component plates (including two flanges and two webs) were investigated in detail. The differences between the residual stresses of NSS, HSS and HNHSS welded box sections were studied. A new model for the residual stress distribution and the corresponding simplified prediction equations defining the residual stress magnitude as a function of the width-to-thickness ratio, steel yield strength, and the plate thickness were proposed for NSS, HSS and HNHSS welded box sections. Good agreement between the predicted results and experimental results was obtained to verify the feasibility of the proposed model.

## 2. Experimental investigation

### 2.1 Cross-section dimensions and material properties

Four different sections were used in this investigation, as illustrated in Fig. 5. The flange and web plates of B-345-10-345-10 are Q345 steel plates with a design thickness of 10 mm, the flange and web plates of B-690-10-690-10 are Q690 steel plates with a design thickness of 10 mm, the web plates of B-345-10-690-10 and B-345-20-690-10 are Q690 steel plates with a design thickness of 10 mm, and the flange plates of B-345-10-690-10 and B-345-20-690-10 are Q345 steel plates with a design thickness of 10 mm and 20 mm, respectively. It should be noted that the column with the section of B-345-20-690-10 could have the same axial bearing capacity as the column with the section of B-690-10-690-10, but the former one has better ductility as indicated in Fig. 3. The details of the design and measured specimen sectional dimensions are listed in Table 1. All the

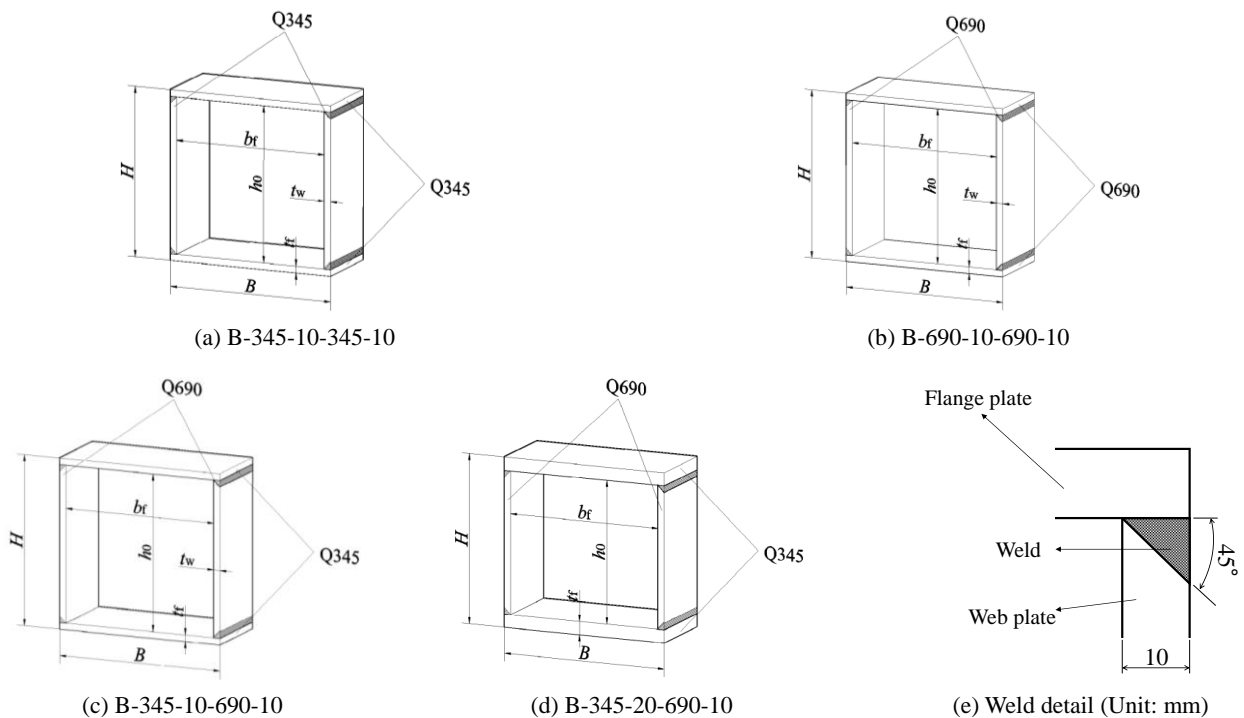


Fig. 5 Shapes and materials of four specimen sections

steel plates were extracted from steel plates with a moderate thickness of 10- or 20-mm using computer numerical control flame cutting technology. Prior to the final butt-welding of the steel specimens, spot welding was initially used to assemble the four steel plates. All the four welds were performed using SMAW, and all the weld sizes were designed to be 10 mm, i.e., equal to the thickness of web plates, as shown in Fig. 5(e).

The material properties of the Q345 and Q690 plates were obtained through tensile coupon tests. A total of nine tensile steel specimens of different grades with different thicknesses were tested. The material properties of steel plates were obtained by calculating the average of the three tensile specimens. Prior to testing, strain gauges were mounted on the tensile specimens to measure the strains. Table 2 summarises the material properties of the tensile test specimens.

## 2.2 Sectioning process

In this study, the residual stresses in four welded box sections were measured using the sectioning method. To maintain the original material properties, an automated electric spark wire-cutting machine (AESWCM) was adopted to ensure that a minimal heat input was introduced into the tested specimens.

The arrangement of the segment specimens cut from a typical box section column is illustrated in Fig. 6. To obtain reliable residual stress results for the entire steel section, the adopted central part had a length of 790 mm (which is more than 3.0 times the minimum value between the width and height of the section). Both ends of the adopted central part were at a distance of at least 400 mm (which is more than 1.5 times the minimum value between the width and height

of the section) from both ends of segment. The number of measurement strips of the sections were 26 in one flange and 24 in one web for B-345-10-345-10, B-690-10-690-10, and B-345-10-690-10 and were 26 in one flange and 22 in one web for B-345-20-690-10. For all the sections, the width of the total strip specimens was fixed at 10 mm. Two holes were mechanically punched into each strip specimen from the outer surface side of section. The design details of the locations of strip specimens with gauge holes are shown in Fig. 7. The distances between each couple of holes for each strip (before and after the release of the residual stress) were measured using the Whittemore strain gauge YB-25 with an initial gauge length of 250 mm and a sensitivity of 0.01 mm, as shown in Fig. 8.

A total of four measurements were conducted throughout the test, by following the sectioning process shown in Fig. 9. Firstly, electric drilling was implemented for punching a couple of holes for each strip, and the initial distance between each couple of holes was measured using the Whittemore strain gauge YB-25 and recorded as  $L_0$ . Secondly, the segment specimens were extracted using AESWCM, and the second distance between each couple of holes after the initial release of the residual stress during this step was measured using the Whittemore strain gauge YB-25 and recorded as  $L_1$ . Using the same technique mentioned above, the flange–web weld fusion line was then separated along the flange–web weld fusion line by employing AESWCM, and the third distance between each couple of holes after the further release of the residual stress during this step was measured using the Whittemore strain gauge YB-25 and recorded as  $L_2$ . Finally, each component plate was evenly divided into strips of a width of 10 mm, and the fourth distance between each couple of holes after the full release of the residual stress during this step was

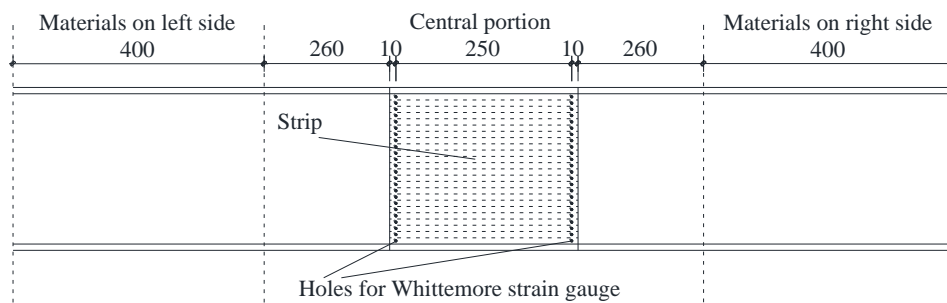


Fig. 6 Arrangement of segment specimens (Unit: mm)

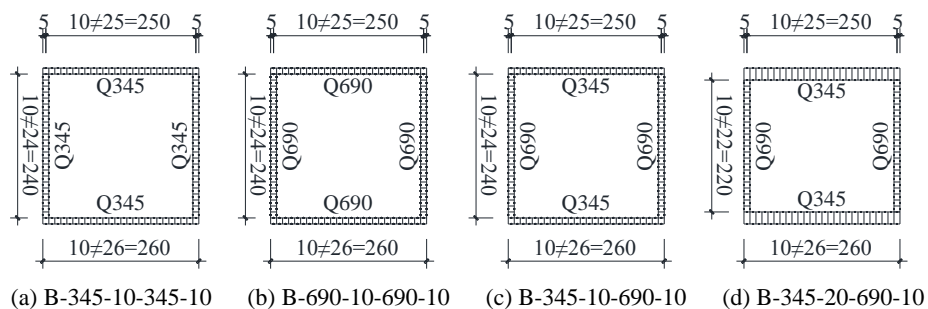


Fig. 7 Arrangement of segment specimens (Unit: mm)



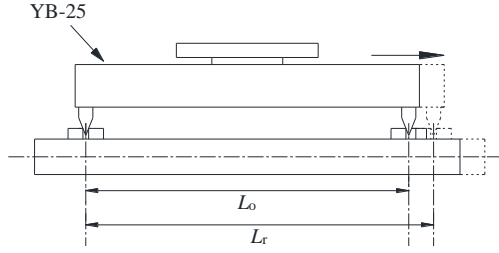


Fig. 8 Measurement of Whittemore strain gauge YB-25

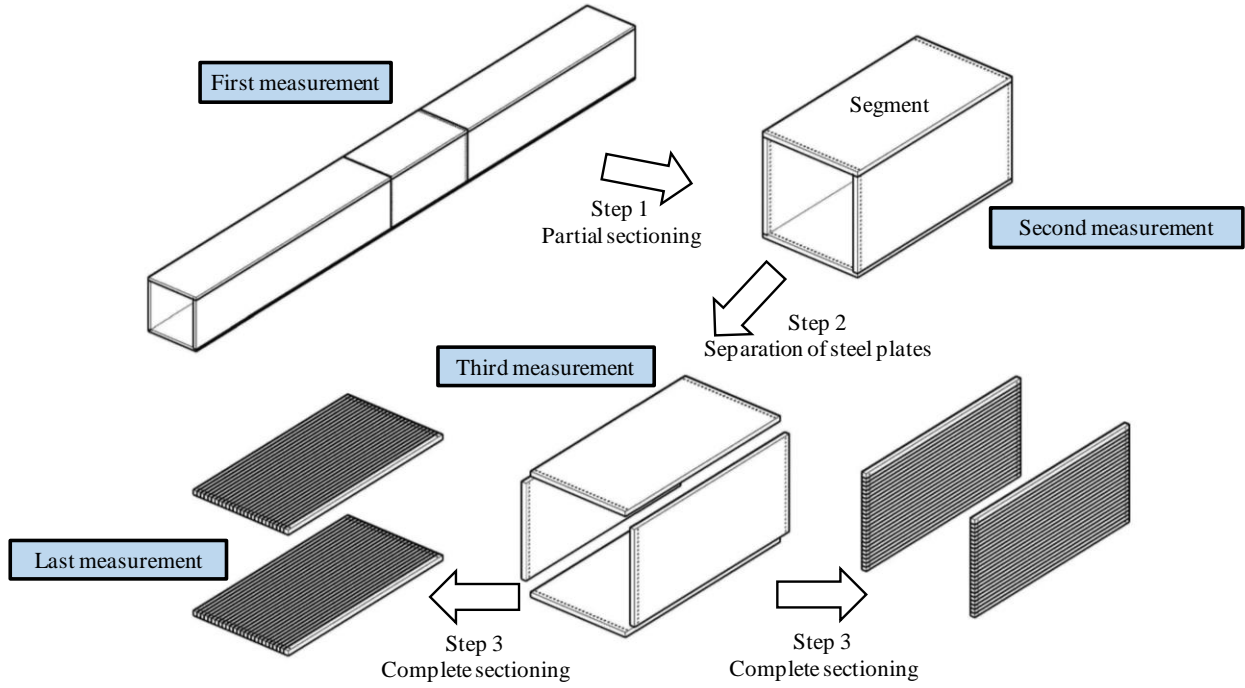


Fig. 9 Sectioning method steps



Fig. 10 Strip specimens after sectioning

measured using the Whittemore strain gauge YB-25 and recorded as  $L_3$ . The strip specimens after the lasting sectioning are presented in Fig. 10. The measured residual strain  $\varepsilon_{r0}$  of each strip after sectioning is given by

$$\varepsilon_{r0} = \frac{L_0 - L_3}{L_3} \quad (1)$$

based on which, the residual stress can be calculated according to Hooke's law.

### 3. Test results and discussions

#### 3.1 Calculation of residual stresses

Owing to the influence of cutting process, the steel strips were bended slightly, so that the measured distance between the two holes was less than the actual distance, as shown in Fig. 11. For each strip, the final lengths measured using the Whittemore strain gauge were chord lengths instead of arc lengths (Yuan *et al.* 2014). It was thus necessary to correct the measured residual strain ( $\varepsilon_{r0}$ ) calculated based on the chord length to the true residual strain ( $\varepsilon_r$ ) obtained based on the arc length. The offset value  $\delta$  and initial gauge length  $L$  of the steel strip are illustrated in Fig. 11. The true residual strain  $\varepsilon_r$  obtained by considering the influence of strip bending can be written as

$$\varepsilon_r = \varepsilon_{r0} - \frac{\left(\frac{\delta}{L}\right)^2}{6\left(\frac{\delta}{L}\right)^4 + 1} \quad (2)$$

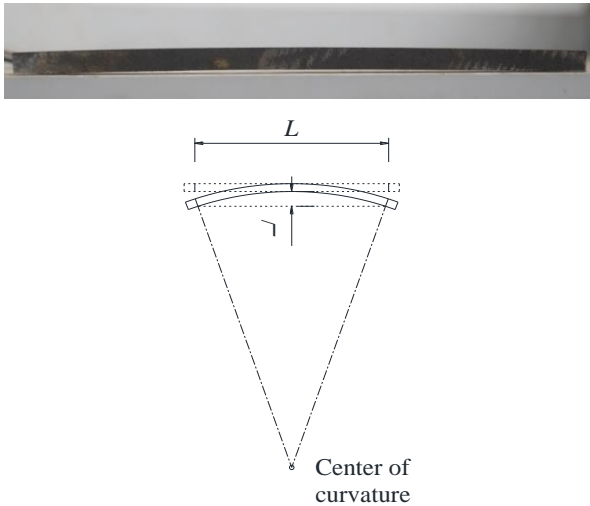
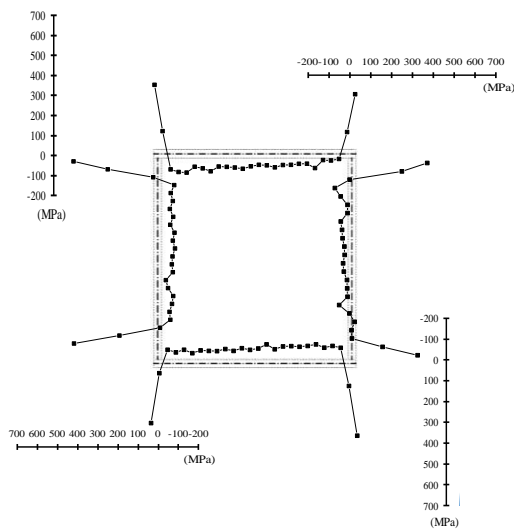


Fig. 11 Longitudinal curvature of strips and definition of curvature offset value  $\delta$

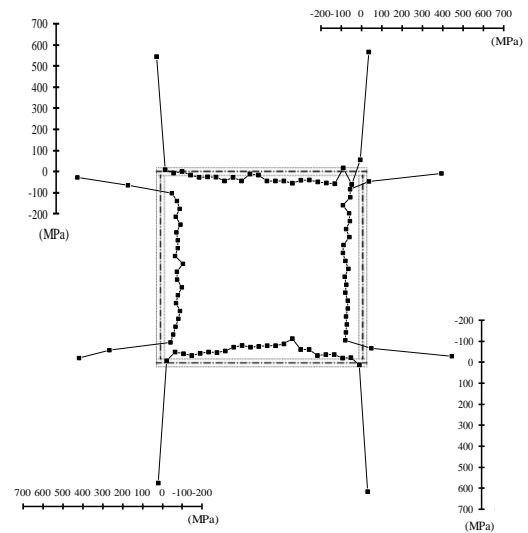
Based on the measured data and the above correction, the magnitudes of the compressive and tensile residual stresses of four welded box section specimens were obtained. The details of the test results of residual stresses for all the sections are shown in Fig. 12.

### 3.2 Residual stress results obtained from tests

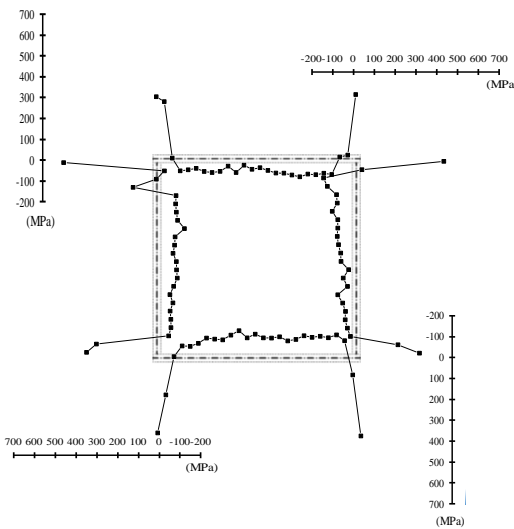
Based on the residual stress results obtained from the above tests, the following general findings were obtained. The distribution pattern of residual stresses for HNHSS box sections is generally similar to that for NSS and HSS box sections. The residual stresses in the area near the welds at the four corners of box sections are in tension, and the substantially constant compressive residual stresses are distributed in the middle of the sectional plates. The distribution pattern of residual stresses is shown in Fig. 13, in a manner similar to the distribution pattern presented by (Ban *et al.* 2013). In Fig. 13,  $\sigma_{rt1}$  to  $\sigma_{rt8}$  are the maximum



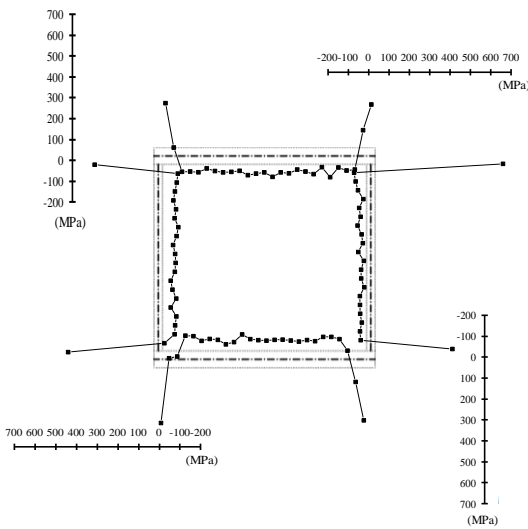
(a) B-345-10-345-10



(b) B-690-10-690-10



(c) B-345-10-690-10



(d) B-345-20-690-10

Fig. 12 Residual stress test results for all sections

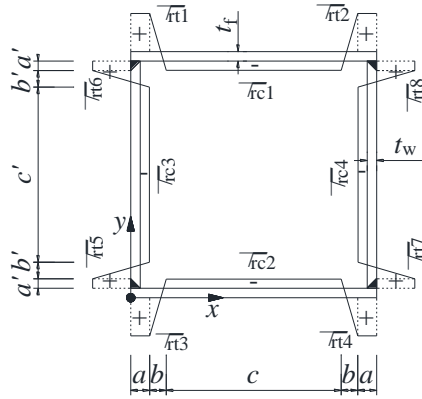


Fig. 13 Distribution pattern of residual stress

magnitudes of the tensile stresses around weld regions,  $\sigma_{rc1}$  and  $\sigma_{rc2}$  are the average magnitudes of the constant compressive stresses for the two flange plates, and  $\sigma_{rc3}$  and  $\sigma_{rc4}$  are the average magnitudes of the constant compressive stresses for the two web plates. The detailed values of the maximum tensile residual stress and average compressive residual stress obtained from the tests are listed in Table 3.

The maximum tensile residual stress ratio ( $\sigma_{rt}/f_y$ ) decreases with the increase in the steel grade and steel plate thickness ( $t_f$  or  $t_w$ ), but has no clear relationship with the plate width-to-thickness ratio ( $b/t_f$  or  $h_0/t_w$ ). As the steel grade increases, the maximum tensile residual stress is much less than its  $f_y$  value which is in contrary to NSS. It can be observed that  $\sigma_{rt}$  of the NSS sections is equal to or close to  $f_y$  of the NSS plate. For the specimen B-345-10-345-10,  $\sigma_{rt}$  changes from  $0.771f_y$  to  $1.089f_y$ , the average magnitude of  $\sigma_{rt}$  is  $0.911f_y$ , which is close to the value of  $f_y$  of the Q345 plate with a design thickness of 10 mm. It can be observed that  $\sigma_{rt}$  of the HSS sections is less than the value of  $f_y$  of the Q690 plate with a design thickness of 10 mm. For the specimen B-690-10-690-10,  $\sigma_{rt}$  ranges from  $0.523f_y$  to  $0.820f_y$ , and the average magnitude of  $\sigma_{rt}$  is  $0.658f_y$ , which is approximately equal to 0.6–0.7 times the value of  $f_y$  of the Q690 plate. Another interesting observation was made: for the NSS section, the maximum

residual stress ratio ( $\sigma_{rt}/f_y$ ) of the web plates (average magnitude of  $\sigma_{rt}/f_y$  of the web plates is 0.979) is on average more than that of the flange plates (average magnitude of  $\sigma_{rt}/f_y$  of the flange plates is 0.843); however, for the HSS section,  $\sigma_{rt}/f_y$  of the web plates (average magnitude of  $\sigma_{rt}/f_y$  of the web plates is 0.557) is on average less than that of the flange plates (average magnitude of  $\sigma_{rt}/f_y$  of the web plates is 0.760). A similar phenomenon was reported in the previous studies (Ban *et al.* 2013, Yuan *et al.* 2014, Cao *et al.* 2018). For the NSS section,  $\sigma_{rt}$  of the flanges is less than that of the webs; however,  $\sigma_{rt}$  of the flanges is more than that of the webs for the HSS sections. The trend of this phenomenon needs to be further confirmed in future tests. In the case of the specimen B-345-10-690-10,  $\sigma_{rt}$  of the Q345 flange plates changes from  $0.772f_y$  to  $0.968f_y$ , and the average magnitude of  $\sigma_{rt}$  is  $0.868f_y$ , which is close to the value of  $f_y$  of the Q345 plate with a design thickness of 10 mm.  $\sigma_{rt}$  of the Q690 web plates ranges from  $0.410f_y$  to  $0.604f_y$ , and the average magnitude of  $\sigma_{rt}$  is  $0.509f_y$ , which is approximately 0.5 times the value of  $f_y$  of the Q690 plate. For the specimen B-345-20-690-10,  $\sigma_{rt}$  of the Q345 flange plates changes from  $0.770f_y$  to  $0.837f_y$ , and the average magnitude of  $\sigma_{rt}$  is  $0.799f_y$ , which is slightly less than that of the specimen B-345-10-690-10.  $\sigma_{rt}$  of the Q690 web plates ranges from  $0.418f_y$  to  $0.880f_y$ , and the average magnitude of  $\sigma_{rt}$  is  $0.609f_y$ , which is slightly more than that of the specimen B-345-10-690-10. The maximum residual stress ratios ( $\sigma_{rt}/f_y$ ) in previous studies (Wang *et al.* 2012, Ban *et al.* 2013, Yuan *et al.* 2014, Li *et al.* 2015, Khan *et al.* 2016, Cao *et al.* 2018, Nie *et al.* 2018, Somodi and Kovesdi 2018) and this study are summarised in Fig. 14. The effects of the steel plate yield strength ( $f_y$ ) and the plate thickness ( $t_f$  or  $t_w$ ) are discussed in the following sections.

In addition, it can be observed that the average compressive residual stress ( $\sigma_{rc}$ ) of the NSS, HSS and HNHSS sections is obviously lower than the yield strength ( $f_y$ ) of the steel plates, and the average compressive residual stress ratio ( $\sigma_{rc}/f_y$ ) of the steel plates decreases with the increase in both the width-to-thickness ratio ( $b/t_f$  or  $h_0/t_w$ ) and  $f_y$  of the steel plates. For the specimen B-345-10-345-10,  $\sigma_{rc}$  changes from  $-0.082f_y$  to  $-0.173f_y$ , and the average magnitude of  $\sigma_{rc}$  is  $-0.154f_y$ . For the specimen B-690-10-

Table 3 Maximum tensile residual stress and average compressive residual stress

Section label	Maximum tensile residual stress								Average compressive residual stress			
	$\sigma_{rt1}$ (MPa)	$\sigma_{rt2}$ (MPa)	$\sigma_{rt3}$ (MPa)	$\sigma_{rt4}$ (MPa)	$\sigma_{rt5}$ (MPa)	$\sigma_{rt6}$ (MPa)	$\sigma_{rt7}$ (MPa)	$\sigma_{rt8}$ (MPa)	$\sigma_{rc1}$ (MPa)	$\sigma_{rc2}$ (MPa)	$\sigma_{rc3}$ (MPa)	$\sigma_{rc4}$ (MPa)
B-345-10-345-10	350.04	303.16	304.97	366.59	427.91	425.23	320.44	366.26	-57.00	-58.00	-68.07	-32.26
B-690-10-690-10	539.86	561.98	579.69	621.19	416.14	424.98	449.20	396.66	-37.07	-51.81	-86.70	-83.73
B-345-10-690-10	303.58	314.01	365.96	380.55	346.08	457.97	310.96	428.85	-58.59	-89.20	-66.39	-73.78
B-345-20-690-10	298.60	292.06	317.34	304.28	447.83	316.85	414.85	666.61	-65.69	-86.33	-77.02	-44.20
	$\sigma_{rt1}/f_y$	$\sigma_{rt2}/f_y$	$\sigma_{rt3}/f_y$	$\sigma_{rt4}/f_y$	$\sigma_{rt5}/f_y$	$\sigma_{rt6}/f_y$	$\sigma_{rt7}/f_y$	$\sigma_{rt8}/f_y$	$\sigma_{rc1}/f_y$	$\sigma_{rc2}/f_y$	$\sigma_{rc3}/f_y$	$\sigma_{rc4}/f_y$
B-345-10-345-10	0.891	0.771	0.776	0.933	1.089	1.082	0.815	0.932	-0.145	-0.148	-0.173	-0.082
B-690-10-690-10	0.712	0.742	0.765	0.820	0.549	0.561	0.593	0.523	-0.049	-0.068	-0.114	-0.110
B-345-10-690-10	0.772	0.799	0.931	0.968	0.457	0.604	0.410	0.566	-0.149	-0.227	-0.088	-0.097
B-345-20-690-10	0.787	0.770	0.837	0.802	0.591	0.418	0.547	0.880	-0.173	-0.228	-0.102	-0.058



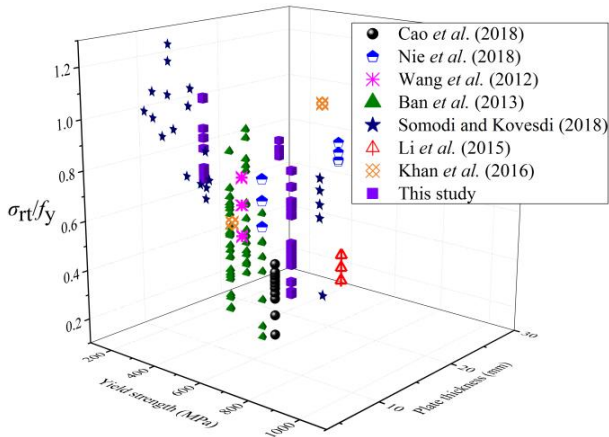


Fig. 14 Maximum tensile residual stress ratio ( $\sigma_{rt}/f_y$ ) in previous studies and this study

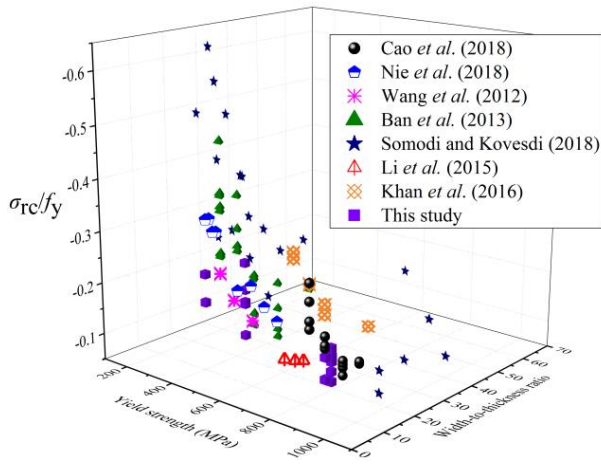


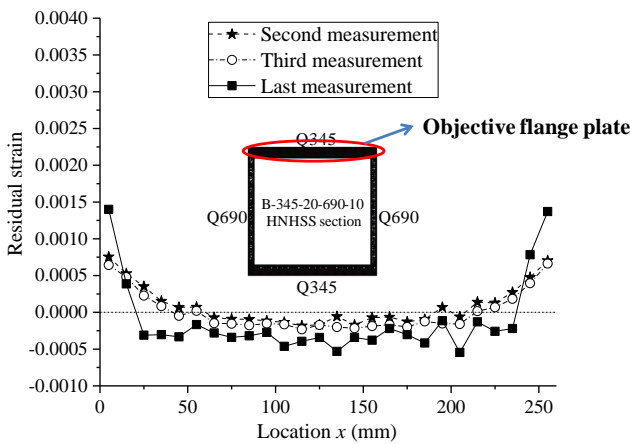
Fig. 15 Average compression residual stress ratio ( $\sigma_{rc}/f_y$ ) in previous studies and this study

690-10,  $\sigma_{rc}$  ranges from  $-0.049f_y$  to  $-0.114f_y$ , and the average magnitude of  $\sigma_{rc}$  is  $-0.086f_y$ , which is less than that of the specimen B-345-10-345-10. This reduction in  $\sigma_{rc}$  is

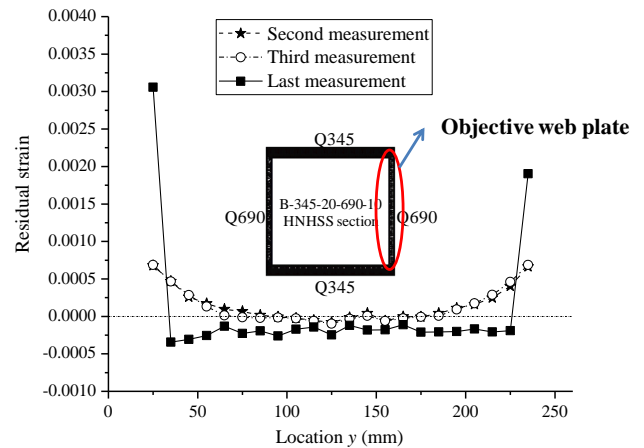
associated with the increase in  $f_y$ . For the specimen B-345-10-690-10,  $\sigma_{rc}$  of the Q345 flange plates with a design thickness of 10 mm changes from  $-0.149f_y$  to  $-0.227f_y$ , and the average magnitude of  $\sigma_{rc}$  is  $-0.188f_y$ , which is slightly more than that of B-345-10-345-10.  $\sigma_{rc}$  of the Q690 web plates changes from  $-0.088f_y$  to  $-0.097f_y$ , and the average magnitude of  $\sigma_{rc}$  is  $-0.092f_y$ , which is a little more than that of B-690-10-690-10. For the specimen B-345-20-690-10,  $\sigma_{rc}$  of the Q345 flange plates with the design thickness of 20 mm ranges from  $-0.173f_y$  to  $-0.228f_y$ , and the average magnitude of  $\sigma_{rc}$  is  $-0.200f_y$ , which is slightly more than that of B-345-10-690-10. The increase in  $\sigma_{rc}$  can be due to the decrease in the width-to-thickness ratio of the flange plate (from 23.38 to 12.07).  $\sigma_{rc}$  of the Q690 web plates changes from  $-0.058f_y$  to  $-0.102f_y$ , and the average magnitude of  $\sigma_{rc}$  is  $-0.080f_y$ , which is a little less than that of B-345-10-690-10. The average compressive residual stress ratios ( $\sigma_{rc}/f_y$ ) in the previous studies (Wang *et al.* 2012, Ban *et al.* 2013, Li *et al.* 2015, Khan *et al.* 2016, Cao *et al.* 2018, Nie *et al.* 2018, Somodi and Kovesdi 2018) and this study are summarised in Fig. 15. The effects of the steel plate yield strength ( $f_y$ ), width-to-thickness ratio ( $b/t_f$  or  $h_0/t_w$ ), and plate thickness ( $t_f$  or  $t_w$ ) of the steel plate are discussed in the following sections.

### 3.3 Process of release of residual stress

To show the process of release of residual stresses during the entire sectioning process, four measurements were performed, as described in Section 2.2. Three residual strains could be obtained during the entire sectioning process. The release trend of the residual stresses (flange and web plate of B-345-20-690-10) is illustrated in Fig. 16. It should be noted that the residual strains of second measurement are slightly less than the residual strains of third measurement, but both these are much less than the residual strain of last measurement. This indicates that the release of residual stresses progress from initial release, to further release, and then to full release. The released tensile residual stresses in the last sectioning are relatively large. This causes a different distribution shape of residual



(a) Changes of residual stress distribution for flange of B-345-20-690-10



(b) Changes of residual stress distribution for web of B-345-20-690-10

Fig. 16 Trend of release of residual stresses (flange and web plate of B-345-20-690-10)

stresses in the last measurement as compared to those of the second and third measurements.

### 3.4 Effect of plate width-to-thickness ratio ( $b/t_f$ or $h_0/t_w$ )

Based on the experimental data shown in Figs. 14 and 15, it can be concluded that the maximum tensile residual stress ratio ( $\sigma_{rt}/f_y$ ) has no clear correlation with the plate width-to-thickness ratio ( $b/t_f$  or  $h_0/t_w$ ), while the average compressive residual stress ratio ( $\sigma_{rc}/f_y$ ) over the middle part of the flange and web plates is significantly related to the width-to-thickness ratio. The relationship between  $\sigma_{rc}/f_y$  and width-to-thickness ratio is shown in Fig. 17, wherein  $\sigma_{rc}/f_y$  in the previous studies (Wang *et al.* 2012, Ban *et al.* 2013, Khan *et al.* 2016, Cao *et al.* 2018, Nie *et al.* 2018, Somodi and Kovesdi 2018) and this study are summarised. In Fig. 17, the cases with the steel plate yield strength ( $f_y$ ) that is less than 450 MPa and more than 690 MPa are denoted in purple and green colours, respectively, while the others are denoted in blue colour. It can be recognised that for given

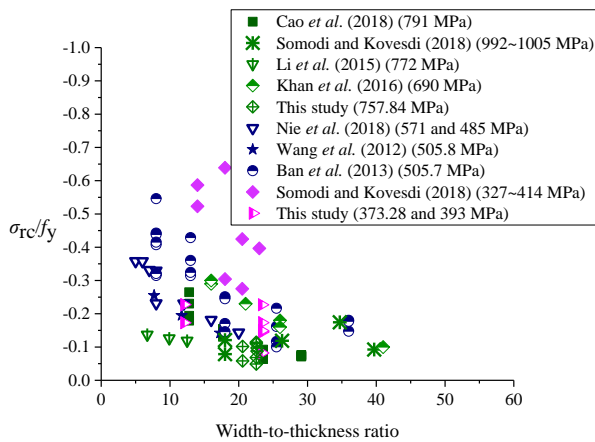
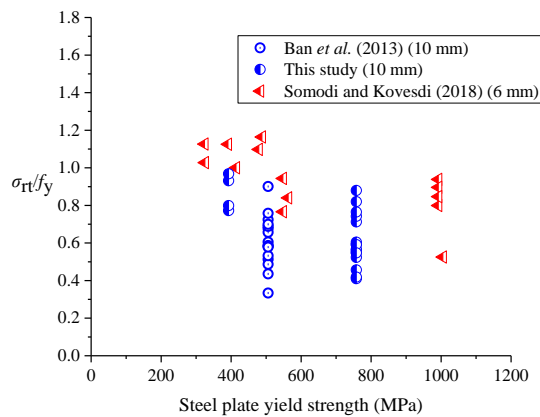


Fig. 17 Relationship between average compression residual stress ratio ( $\sigma_{rc}/f_y$ ) and width-to-thickness ratio ( $b/t_f$  or  $h_0/t_w$ )



(Plate thickness is 6 mm as indicated in red and 10 mm as indicated in blue)

Fig. 18 Relationship between maximum tensile residual stress ratio ( $\sigma_{rt}/f_y$ ) and steel plate yield strength ( $f_y$ )

values of  $f_y$ ,  $\sigma_{rc}/f_y$  decreases with an increase in the width-to-thickness ratio of the component plates when the width-to-thickness ratio is less than 25. This decrease ratio of the  $\sigma_{rc}/f_y$  to plate width-to-thickness ratio reduces as  $f_y$  increases. When the width-to-thickness ratio is more than 25, this trend is not obvious.

### 3.5 Effect of steel plate yield strength ( $f_y$ )

Based on the experimental data shown in Figs. 14 and 15, it can be concluded that both the maximum tensile residual stress ratio ( $\sigma_{rt}/f_y$ ) and average compressive residual stress ratio ( $\sigma_{rc}/f_y$ ) are significantly associated with the steel-plate yield strength ( $f_y$ ). The relationship between  $\sigma_{rt}/f_y$  and  $f_y$  is shown in Fig. 18, in which  $\sigma_{rt}/f_y$  in the previous studies (Ban *et al.* 2013, Somodi and Kovesdi 2018) and this study are summarised. Only the cases comprising plate thickness of 6 mm and 10 mm are included in Fig. 18. It can be seen from Fig. 18 that  $\sigma_{rt}/f_y$  decreases with the increase in  $f_y$  when  $f_y$  is less than 600 MPa. This trend is not obvious when  $f_y$  is more than 600 MPa. When  $f_y$  is less than 500 MPa,  $\sigma_{rt}/f_y$  may be more than 1.0 in some cases, but  $\sigma_{rt}/f_y$  is always less than 1.0 when  $f_y$  is more than 500 MPa. In this study, the average magnitude of the maximum tensile residual stress ratio ( $\sigma_{rt}/f_y$ ) of the Q345 plates including four plates of B-345-10-345-10 and two flange plates of B-345-10-690-10 is 0.897, which is significantly more than the average magnitude (0.642) of  $\sigma_{rt}/f_y$  of the Q690 plates including the four plates of B-690-10-690-10, two web plates of B-345-10-690-10, and two web plates of B-345-20-690-10.

The relationship between  $\sigma_{rc}/f_y$  and  $f_y$  is shown in Fig. 19, in which  $\sigma_{rc}/f_y$  obtained from previous studies (Ban *et al.* 2013, Cao *et al.* 2018, Nie *et al.* 2018, Somodi and Kovesdi 2018) and this study are summarised. Only the cases with the width-to-thickness ratio ranged from 20 and 26 are included in Fig. 19. It can be observed from Fig. 19 that  $\sigma_{rc}/f_y$  decreases with the increase in  $f_y$  when  $f_y$  is less than 600 MPa, and this trend is not obvious when  $f_y$  is more than 600 MPa.

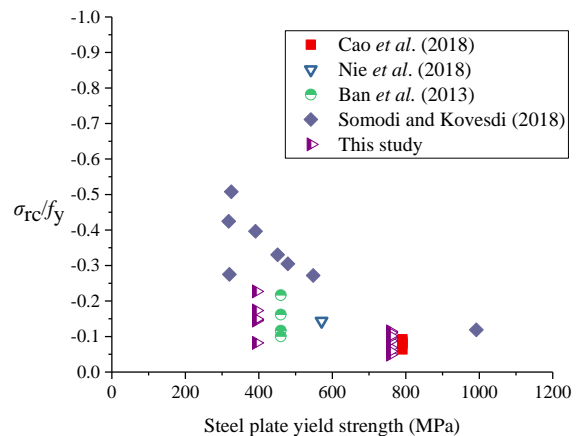


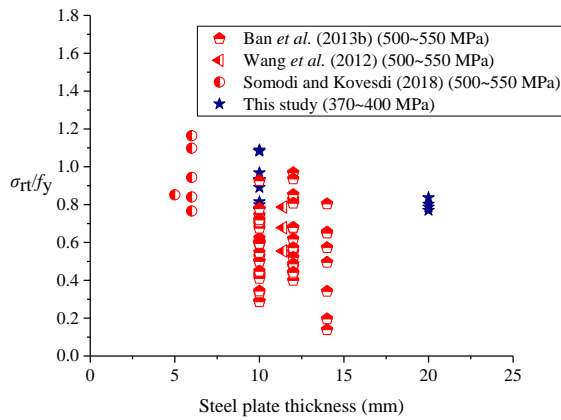
Fig. 19 Relationship between average compression residual stress ratio ( $\sigma_{rc}/f_y$ ) and steel plate yield strength ( $f_y$ )

### 3.6 Effect of plate thickness ( $t_f$ or $t_w$ )

It can be concluded that the maximum tensile residual stress ratio ( $\sigma_{rt}/f_y$ ) is significantly correlated with the steel plate thickness ( $t_f$  or  $t_w$ ), based on the experimental data shown in Figs. 14 and 15. The relationship between  $\sigma_{rt}/f_y$  and the steel plate thickness is illustrated in Fig. 20, in which the cases of steel plates with yield strength ( $f_y$ ) as 370–400 MPa and 500–550 MPa are indicated in blue and red colour, respectively. It can be observed that  $\sigma_{rt}/f_y$  decreases with the increase in the steel plate thickness.

### 3.7 Discussion on HNHSS box sections (B-345-10-690-10 and B-345-20-690-10)

For the HNHSS welded box sections, when the thickness of the flange plate is equal to that of the web plate (B-345-10-690-10), the maximum tensile residual stress ( $\sigma_{rt}$ ) of the Q345 flange plate is a little less than the yield strength ( $f_y$ ), which is slightly less than the average magnitude of  $\sigma_{rt}$  of four Q345 steel plates for the specimen B-345-10-345-10. The  $\sigma_{rt}$  of the Q690 web plate is significantly less than  $f_y$ , which is slightly more than the average magnitude of  $\sigma_{rt}$  of four Q690 steel plates for the specimen B-690-10-690-10. Furthermore, as is shown in Table 3, the maximum residual stress ratios ( $\sigma_{rt}/f_y$ ) of B-345-20-690-10 are more evenly distributed on the section



(Steel plate yield strength is 370–400 MPa as indicated in blue and 500–550 MPa as indicated in red)

Fig. 20 Relationship between maximum tensile residual stress ratio ( $\sigma_{rt}/f_y$ ) and steel plate thickness ( $t_f$  or  $t_w$ )

than those of B-345-10-690-10. The previous research has found that the residual stress magnitude was associated with the heat input rather than the weld size (Rasmussen and Hancock 1988). Table 4 presents the values of  $(\sigma_{rt}/f_y)_f/(\sigma_{rt}/f_y)_w$  and  $f_{y,f} \cdot t_f/f_{y,w} \cdot t_w$  for four tested sections. For the specimens B-345-10-345-10, B-690-10-690-10, and B-345-20-690-10, because  $f_{y,w} \cdot t_w$  of the web plate is equal to  $f_{y,f} \cdot t_f$  of the flange plate, the heat inputs in the flange and web plates of these specimens could be relatively similar, which lead to close values between  $(\sigma_{rt}/f_y)_f$  and  $(\sigma_{rt}/f_y)_w$ . For the specimen B-345-10-690-10, the heat inputs in the web plates could be more than that in the flange plates since the magnitudes of  $f_{y,w} \cdot t_w$  are significantly greater than those of  $f_{y,f} \cdot t_f$ , so higher values of  $(\sigma_{rt}/f_y)_f/(\sigma_{rt}/f_y)_w$  can be identified.

### 3.8 Self-equilibrium

Owing to the absence of external forces acting on the specimens, the summation of internal force of entire steel section should theoretically be zero. However, in practice, the unbalanced sectional stress may exist because of the inevitable existence of measurement error. To evaluate the accuracy of the residual stress measurements, the self-balancing deviation stress  $\sigma_{err}$  is defined as follows

$$\sigma_{err} = \frac{[\sum_{i=1}^n A_i \cdot \sigma_{ri}]}{A} \quad (3)$$

where  $A$  and  $A_i$  denote the cross-section area of the entire

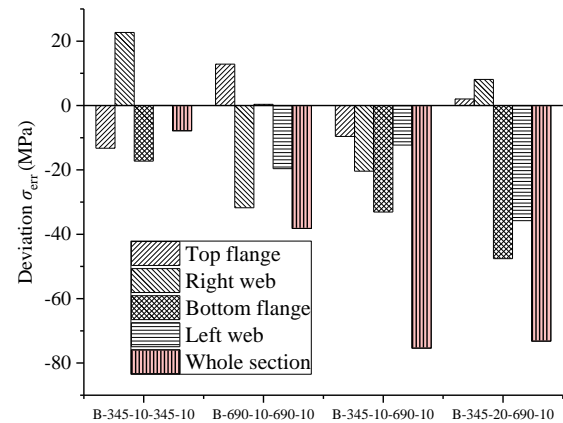


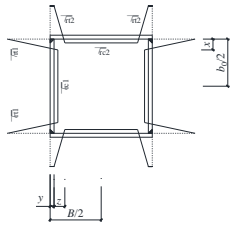
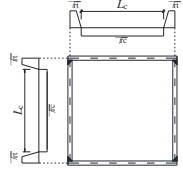
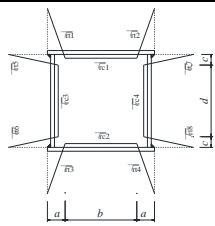
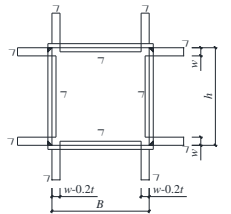
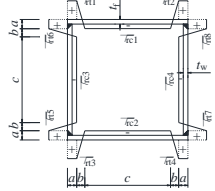
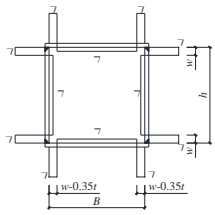
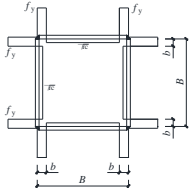
Fig. 21 Self-balancing deviation stresses of flanges, webs and entire sections

Table 4 Relationship between  $(\sigma_{rt}/f_y)_f/(\sigma_{rt}/f_y)_w$  and  $f_{y,f} \cdot t_f/f_{y,w} \cdot t_w$

Section label	$(\sigma_{rt}/f_y)_f$	$(\sigma_{rt}/f_y)_w$	Flange yield strength $f_{y,f}$ (MPa)	Web yield strength $f_{y,w}$ (MPa)	Flange thickness $t_f$ (mm)	Web thickness $t_w$ (mm)	$f_{y,f} \cdot t_f/f_{y,w} \cdot t_w$	$(\sigma_{rt}/f_y)_f/(\sigma_{rt}/f_y)_w$
B-345-10-345-10	0.843	0.979	393.04	393.04	10.18	10.10	1.008	0.861
B-690-10-690-10	0.760	0.557	757.84	757.84	10.60	10.59	1.001	1.364
B-345-10-690-10	0.868	0.509	393.04	757.84	10.17	10.60	0.498	1.705
B-345-20-690-10	0.799	0.609	379.28	757.84	19.98	10.63	0.941	1.312

\*Notes:  $(\sigma_{rt}/f_y)_f$  represents the average magnitude of maximum residual stress ratios of flange plates;  $(\sigma_{rt}/f_y)_w$  represents the average magnitude of maximum residual stress ratios of web plates

Table 5 Previous residual stress models for HSS box sections

Reference	Steel grade, welding details	Plate thickness $t$ (mm)	Models	Simplified prediction equations
Nie <i>et al.</i> (2018)	Q460GJ, CO2 gas-shielded welding	12		$\sigma_{rt1} = 0.93f_y, \sigma_{rt2} = 0.87f_y, \sigma_{rc1} = 2.98 \frac{h_0}{t} - 169.3,$ $\sigma_{rc2} = \frac{3.13h_0}{t} - 137.8 \left(1 \leq \frac{h_0}{t} \leq 43\right)$
		25		$\sigma_{rt1} = 0.85f_y, \sigma_{rt2} = 0.76f_y, \sigma_{rc1} = 12.31 \frac{h_0}{t} - 228.7,$ $\sigma_{rc2} = \frac{27.48h_0}{t} - 373.2 \left(1 \leq \frac{h_0}{t} \leq 13\right)$
Somodi and Kövesdi (2018)	S235-S960 metal active gas welding	$\leq 5$		$\sigma_{rt} = f_y$ $\sigma_{rc} = 70 - 21t + t^2 - \frac{[2900 - 3600 \cdot (t - 5)]}{(h/t)}$
		$> 5$		$\sigma_{rt} = f_y$ $\sigma_{rc} = 70 - 21t + t^2 - \frac{[2900 - 290 \cdot (t - 5)]}{(h/t)}$
Cao <i>et al.</i> (2018)	800 MPa, gas shielded arc welding	7		$\sigma_{rt} = f_y$ $\sigma_{rc} = -4100 + 25 \cdot (h_0/t) - 0.45 \cdot (h_0/t)^2$
Li <i>et al.</i> (2015)	Q690, manual gas metal arc welding	16		$\sigma_{rt} = (0.394 \sim 0.496)f_y$ $\sigma_{rc} = (-0.137 \sim -0.119)f_y$
Ban <i>et al.</i> (2013)	Q460, manual metal arc welding	10, 12, 14		$\sigma_{rt} = f_y$ $\sigma_{rc} = -10 - \frac{1500}{\left(\frac{h_0}{t}\right)} - \frac{550}{t}$ $(-460 \text{ MPa} \leq \sigma_{rc} \leq -46 \text{ MPa})$
Wang <i>et al.</i> (2012)	Q460, manual gas metal arc welding	12		$\sigma_{rt} = (0.555 \sim 0.787)f_y$ $\sigma_{rc} = (-0.255 \sim -0.142)f_y$
Khan <i>et al.</i> (2016)	Q690, gas metal arc welding	5, 16		$\sigma_{rt} = f_y, \sigma_{rc} = - \left[ 3.6607 \left( \frac{B}{t} \right)^{-0.924} \right] f_y$ $b = \frac{-B\sigma_{rc}}{2(\sigma_{rt} - \sigma_{rc})}$

\* Note:  $t$  is the plate thickness,  $h_0/t$  is the width-to-thickness ratio of plate

steel plate and a strip, respectively;  $n$  is the amount of strip specimens of steel plate; and  $\sigma_{ri}$  denotes the residual stress magnitude of each strip. The positive value represents the

tensile residual stress, and the negative value represents the compressive ones. Self-balancing deviation stresses of the flanges, webs, and entire sections are shown in Fig. 21.

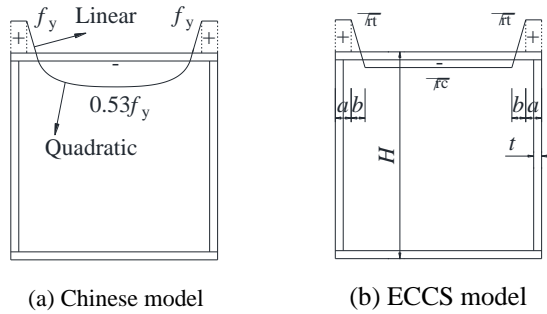


Fig. 22 Present residual stress models for NSS welded box sections

It can be seen that the self-balancing deviation stress  $\sigma_{err}$  of the entire section obtained by integral summation is almost negative and its absolute value is much less than the yield strength  $f_y$ . As the deviation stress was less than 6% of the yield strength for each steel plate, the flange and web plates could be regarded as self-balancing.

#### 4. Models of residual stresses for NSS, HSS, and HNHSS welded box sections

##### 4.1 Previous models of residual stresses for NSS and HSS welded box sections

The residual stress models for NSS welded box sections have been provided in some design codes, including Chinese Steel Structure Code GB50017-2017 (2017) and European Convention for Constructional Steelwork (ECCS) (1976). Two typical models: the Chinese model and ECCS model are illustrated in Fig. 22. For the Chinese model, the maximum tensile residual stress ( $\sigma_{rt}$ ) was equal to the yield strength ( $f_y$ ), and the distribution function of the compressive residual stress ( $\sigma_{rc}$ ) was a quadratic function, in which the maximum compressive residual stress was equal to  $0.53f_y$ . Moreover, the effects of the sectional dimensions have been considered in the determination of the distribution range of the tensile residual stress around the weld region, and no specified compressive stress distribution range was given (Ban *et al.* 2013). On the other hand, for the ECCS model, the distribution ranges were given based on the width-to-thickness ratio, the average magnitude of compressive residual stress could be calculated

according to the plate width-to-thickness ratio and welding type, and the maximum tensile residual stress was assumed to be constant being equivalent to the steel yield strength ( $f_y$ ).

Previous residual stress models (Wang *et al.* 2012, Ban *et al.* 2013, Li *et al.* 2015, Khan *et al.* 2016, Cao *et al.* 2018, Nie *et al.* 2018, Somodi and Kovesdi 2018) for HSS welded box sections are summarised in Table 5. The effect of the difference between the maximum tensile residual stresses of the flange and web is considered only in the residual stress model in (Nie *et al.* 2018). The detailed weld position of the box sections in (Cao *et al.* 2018) is different from that of the other experimental studies. The residual stress model in (Li *et al.* 2015) is similar to that in (Wang *et al.* 2012) while both the maximum tensile residual stress and average compressive residual stress regions in these two models are different. The residual stress model in (Somodi and Kovesdi 2018) is similar to that in (Ban *et al.* 2013), whereas the transition regions from tensile residual stress to compressive residual stress in these two models are slightly different. In fact, the residual stress model in (Ban *et al.* 2013) can almost cover other residual stress models in previous references (Wang *et al.* 2012, Li *et al.* 2015, Khan *et al.* 2016, Cao *et al.* 2018, Somodi and Kovesdi 2018) by changing the parameters of this model. In Table 6, the comparison between tested results in this study and prediction results obtained by previous models based on NSS's residual stress model from Chinese Steel Structure Code GB50017-2017 (2017) and HSS's residual stress model in (Li *et al.* 2015) for grade 690 steel. However, the prediction results from previous model are quite different with test results. Consequently, previous distribution models for the NSS and HSS welded box sections cannot be employed for HNHSS welded box sections based on the data listed in Table 6.

##### 4.2 Proposed model of residual stresses for NSS, HSS, and HNHSS welded box sections

Based on the test results of this study as shown in Fig. 12, and those of previous studies (Wang *et al.* 2012, Ban *et al.* 2013, Li *et al.* 2015, Khan *et al.* 2016, Cao *et al.* 2018, Nie *et al.* 2018, Somodi and Kovesdi 2018), a residual stress model as shown in Fig. 23 is proposed in this study. This proposed model is an improved model based on Ban's model (Ban *et al.* 2013) and can be employed for NSS, HSS and HNHSS welded box sections. The main differences between the proposed model and the Ban's model are

Table 6 Comparison between tested results in this study and prediction results obtained by previous model

Section label		Maximum tensile residual stress								Average compressive residual stress			
		$\sigma_{rt1}$ (MPa)	$\sigma_{rt2}$ (MPa)	$\sigma_{rt3}$ (MPa)	$\sigma_{rt4}$ (MPa)	$\sigma_{rt5}$ (MPa)	$\sigma_{rt6}$ (MPa)	$\sigma_{rt7}$ (MPa)	$\sigma_{rt8}$ (MPa)	$\sigma_{rc1}$ (MPa)	$\sigma_{rc2}$ (MPa)	$\sigma_{rc3}$ (MPa)	$\sigma_{rc4}$ (MPa)
B-345-10-690-10	Test	303.58	314.01	365.96	380.55	346.08	457.97	310.96	428.85	-58.59	-89.20	-66.39	-73.78
	Previous model	393.04	393.04	393.04	393.04	378.92	378.92	378.92	378.92	-208.31	-208.31	-90.94	-90.94
B-345-20-690-10	Test	298.60	292.06	317.34	304.28	447.83	316.85	414.85	666.61	-65.69	-86.33	-77.02	-44.20
	Previous model	379.28	379.28	379.28	379.28	378.92	378.92	378.92	378.92	-201.02	-201.02	-90.94	-90.94



described as follows:

- (1) The maximum magnitude of tensile residual stress of flange plates may be different from that of web plates, and the distribution region of tensile residual stress of flange plates may be different from that of web plates.
- (2) The average magnitude of compressive residual stress of flange plates may be different from that of web plates, and the distribution region of compressive residual stress of flange plates may be different from that of web plates.
- (3) The maximum magnitude of tensile residual stress of the flange and web plates may be less than the yield strength ( $f_y$ ) and can be determined based on the yield strength and thickness of the plate.
- (4) The proposed model can be employed not only for NSS and HSS box sections but also for HNHSS box sections.

The relationship of the geometric parameters shown in Fig. 23 can be described as follows

$$2a + 2b + c = B \quad (4)$$

$$2a' + 2b' + c' = h_0 \quad (5)$$

where  $B$  is the flange width and  $h_0$  is the web height as shown in Fig. 5, and both values of  $a$  and  $a'$  are determined

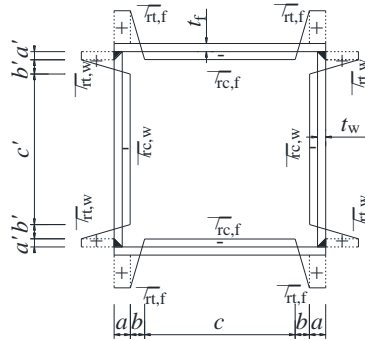


Fig. 23 Model proposed in this study

by choosing the minimum value of  $t_f$  and  $t_w$ .

The residual stress equilibrium was satisfied for each component steel plate and could be written as follows

$$\iint_{A_f} \sigma_{r,f} dA = 0 \quad \text{for flange plate} \quad (6)$$

$$\iint_{A_w} \sigma_{r,w} dA = 0 \quad \text{for web plate} \quad (7)$$

where  $A_f$  and  $A_w$  denote the cross-sectional areas of the flange and web, respectively; and  $\sigma_{r,f}$  and  $\sigma_{r,w}$  are the residual stresses of the flange and web, respectively. Eqs. (6) and (7) can also be rewritten as follows

$$(2a + b) \cdot \sigma_{rt,f} = c \cdot |\sigma_{rc,f}| \quad \text{for flange plate} \quad (8)$$

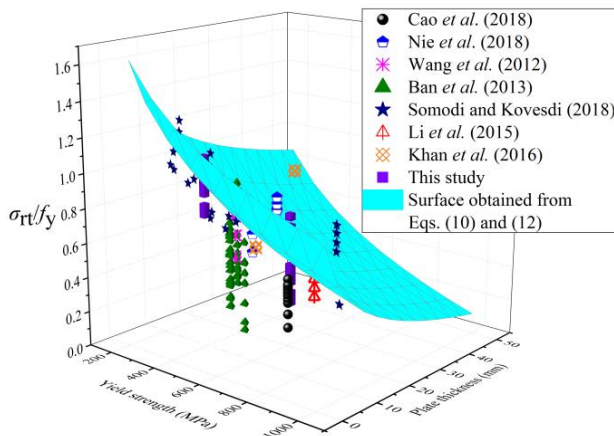
$$(2a' + b') \cdot \sigma_{rt,w} = c' \cdot |\sigma_{rc,w}| \quad \text{for web plate} \quad (9)$$

where  $\sigma_{rt,f}$  and  $\sigma_{rc,f}$  are the tensile residual stress and compressive residual stress of the flange plates, respectively; and  $\sigma_{rt,w}$  and  $\sigma_{rc,w}$  are the tensile residual stress and compressive residual stress of the web plates, respectively.

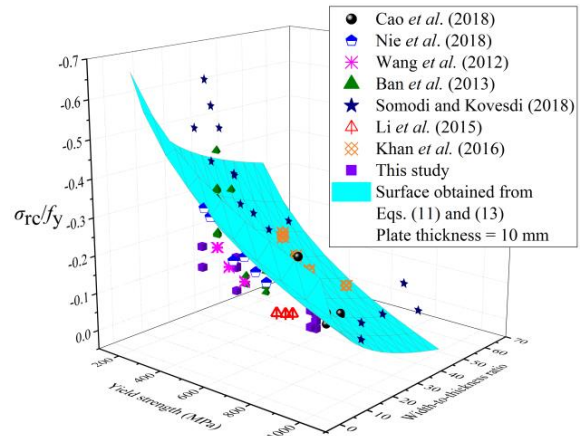
Based on the experimental results of 55 specimens, including 45 specimens from previous studies (Wang *et al.* 2012, Ban *et al.* 2013, Li *et al.* 2015, Khan *et al.* 2016, Cao *et al.* 2018, Nie *et al.* 2018, Somodi and Kovesdi 2018) and four specimens in this study (as shown in Figs. 14 and 15), as well as by using nonlinear surface fitting as shown in Fig. 24, the equations for predicting the maximum tensile residual stress ratio ( $\sigma_{rt,f}/f_{y,f}$  or  $\sigma_{rt,w}/f_{y,w}$ ) and average compressive residual stress ratio ( $\sigma_{rc,f}/f_{y,f}$  or  $\sigma_{rc,w}/f_{y,w}$ ) of the steel plates can be obtained as follows

$$\frac{\sigma_{rt,f}}{f_{y,f}} = 31.850 - 15.400f_{y,f}^{0.0260} - 12.400t_f^{0.0180} \quad (10)$$

$$\frac{\sigma_{rc,f}}{f_{y,f}} = -16.900 + 10.125f_{y,f}^{0.0212} + 4.833 \left( \frac{b_f}{t_f} \right)^{0.0195} + \frac{t_f^2}{20000} \quad (11)$$



(a) Maximum tensile residual stress



(b) Average compressive residual stress

Fig. 24 Proposed fitting surfaces for experimental data

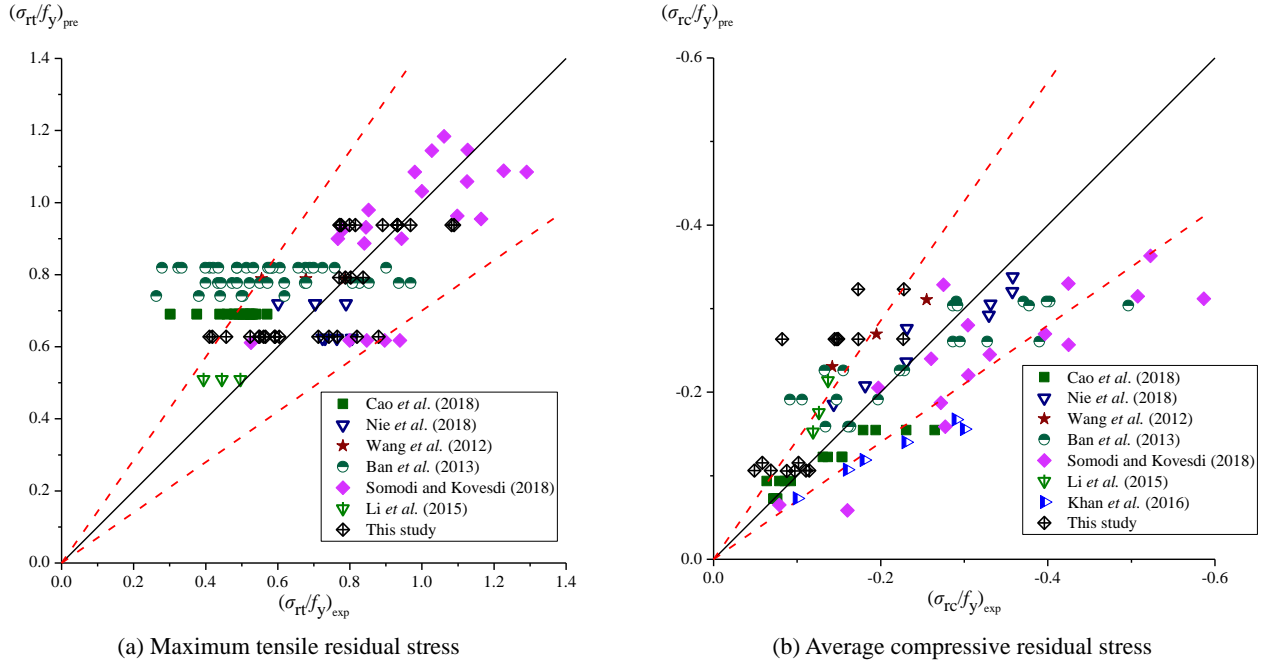


Fig. 25 Comparison of predicted and test results of residual stresses

$$\frac{\sigma_{rt,w}}{f_{y,w}} = 31.850 - 15.400f_{y,w}^{0.0260} - 12.400t_w^{0.0180} \quad (12)$$

$$\begin{aligned} \frac{\sigma_{rc,w}}{f_{y,w}} = & -16.900 + 10.125f_{y,w}^{0.0212} \\ & + 4.833\left(\frac{h_0}{t_w}\right)^{0.0195} + \frac{t_w^2}{20000} \end{aligned} \quad (13)$$

where  $f_{y,f}$  and  $f_{y,w}$  are the yield strengths of the flange and

web, respectively. Fig. 25 depicts the comparison of the results predicted by using the residual stress model proposed in this study and the test results for the maximum tensile residual stress and average compressive residual stress.  $(\sigma_{rt}/f_y)_{pre}$  and  $(\sigma_{rt}/f_y)_{exp}$  are the maximum tensile residual stress ratio predicted by using the model proposed in this study and that obtained from the tests, respectively;  $(\sigma_{rc}/f_y)_{pre}$  and  $(\sigma_{rc}/f_y)_{exp}$  are the average compressive residual stress ratio predicted by the model proposed in this study and that obtained from tests, respectively. Prediction error

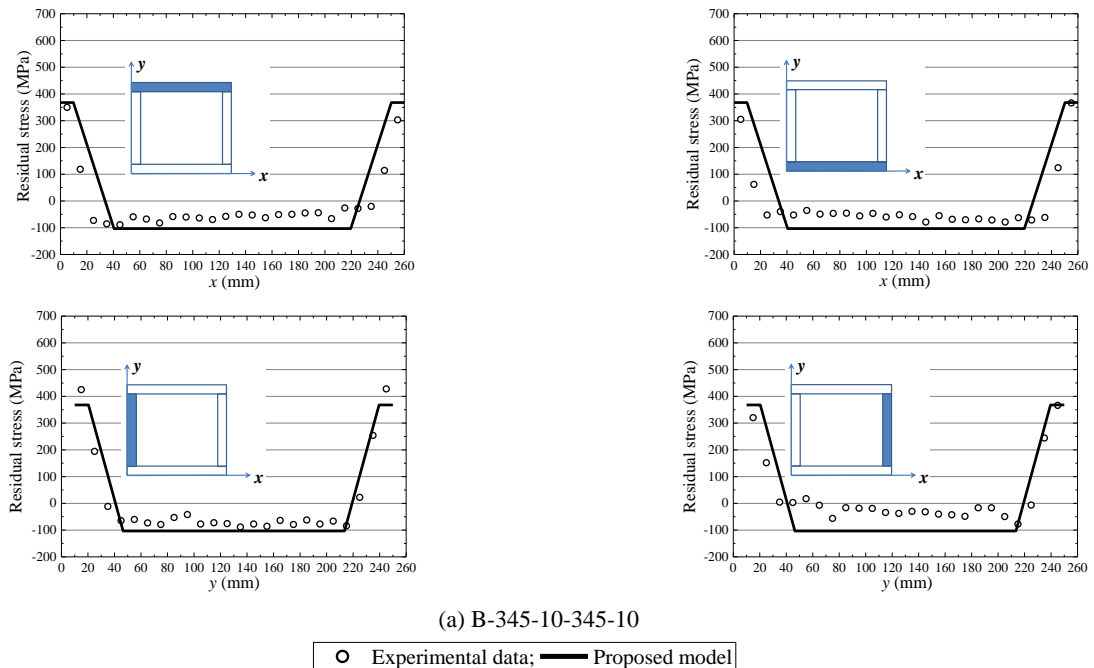


Fig. 26 Comparison of predicted and test results of residual stress magnitudes and distributions

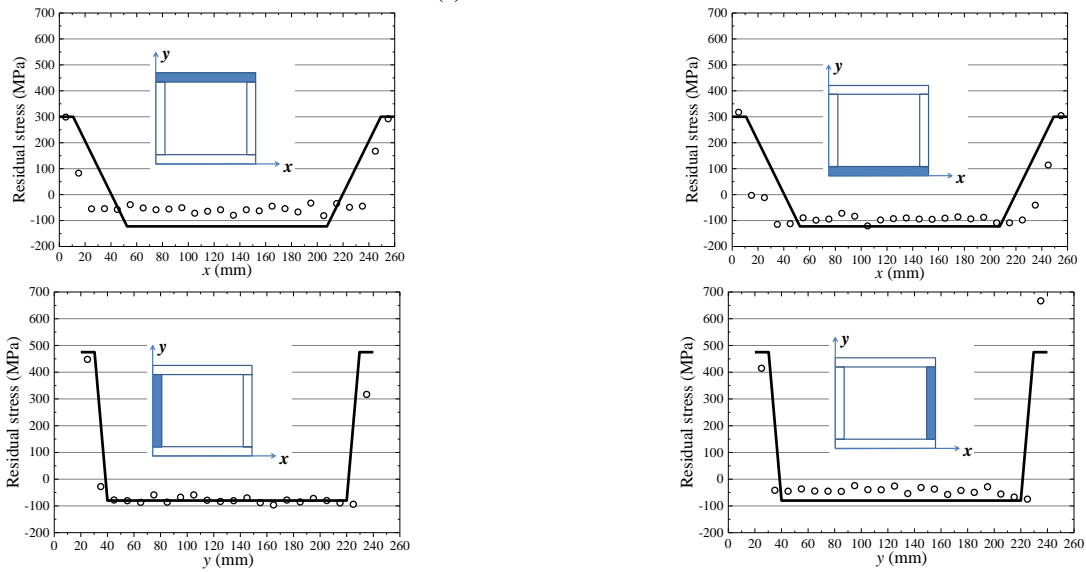
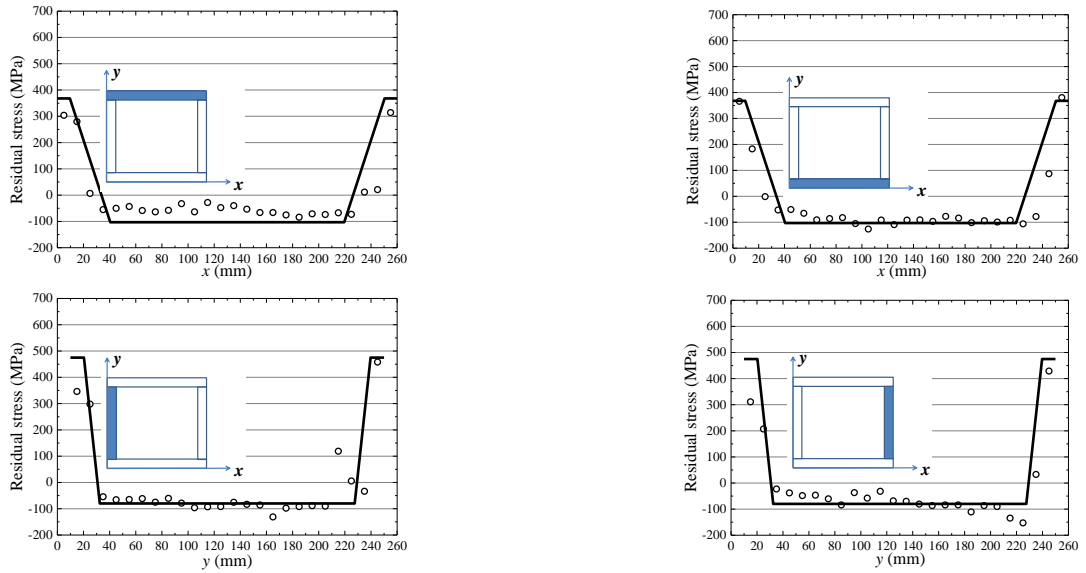
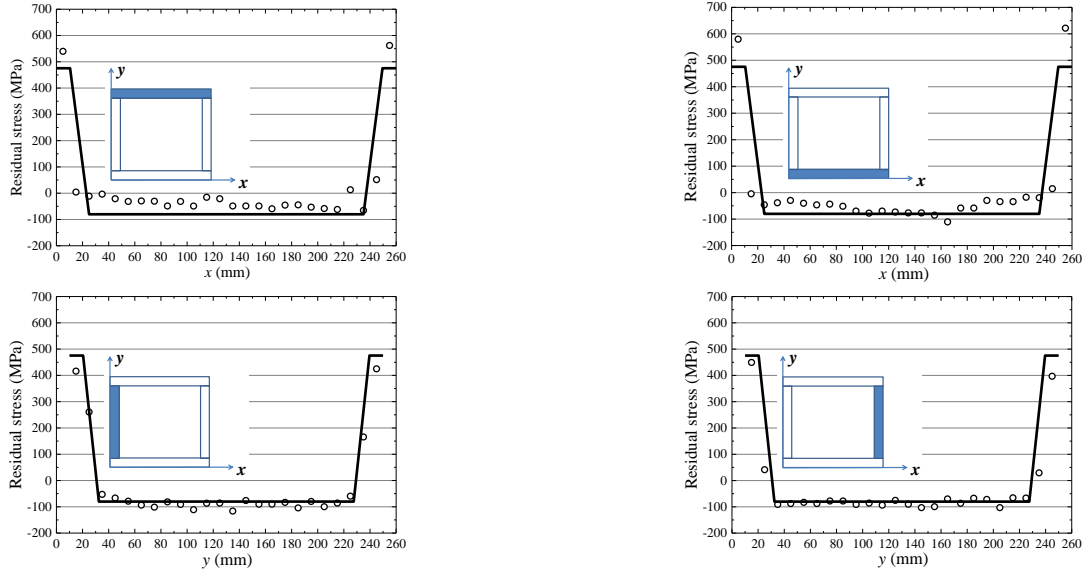


Fig. 26 Continued

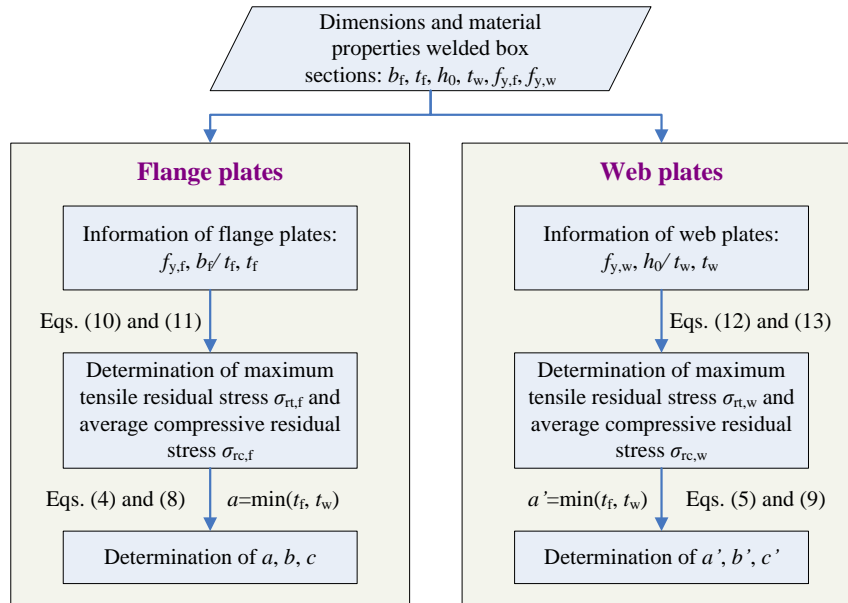


Fig. 27 Flowchart of determination of residual stress magnitudes and distributions of NSS, HSS and HNHSS welded box sections

boundaries of  $\pm 30\%$  are also plotted in Fig. 25. Apparently, it is shown from Fig. 25 that most of the data points are located between the  $\pm 30\%$  margin lines. The residual stress test is a random testing procedure with great randomness. Some data points are outside the  $\pm 30\%$  margin lines because the residual stress magnitude and distribution are influenced by various factors, such as weld type, welding process, measurement error, and weld quality. However, the prediction formula in Fig. 25(a) is only related to yield strength and plate thickness, and the prediction formula in Fig. 25(b) is just related to yield strength and width-to-thickness ratio. There may be other factors that are not reflected in these formulas. These other affected factors may lead to the discreteness of the experimental results compared with the prediction results. Therefore, it is demonstrated that the proposed equations provide a good prediction for the calculation of the values of  $\sigma_{rt,f}$ ,  $\sigma_{rc,f}$ ,  $\sigma_{rt,w}$  and  $\sigma_{rc,w}$ .

Fig. 26 shows the comparison of the results of residual stress magnitudes and distributions predicted by the proposed model and the test results obtained in this study. The detailed process of determination of the residual stress magnitudes and distributions of the welded box sections is presented in Fig. 27. It is shown from Fig. 26 that the predicted residual stress results obtained by using the proposed model agree well with the experimental results of NSS, HSS, and HNHSS welded box sections in this study, which indicates that the proposed residual model estimates the residual stresses with a relatively high accuracy.

## 5. Conclusions

The residual stresses of four box sections including one NSS box section, one HSS box section, and two HNHSS box sections were experimentally investigated in this study. Based on the residual stress test results, the effects of the

width-to-thickness ratio, steel plate yield strength and the plate thickness on the residual stresses of NSS, HSS and HNHSS welded box sections were studied. A residual stress model that can be employed for NSS, HSS and HNHSS welded box sections and the corresponding simplified prediction equations were proposed based on the test data obtained from previous studies and this study. A comparison of the results predicted by the proposed residual stress model and the experimental results was undertaken for validation purposes. Based on these discussions, the conclusions are as follows:

- (1) The distribution shape and features of the residual stresses for HNHSS welded box sections were very similar to those of the NSS and HSS welded box sections.
- (2) The maximum magnitude of the tensile residual stresses around the welds in the flanges and webs was not a fixed value as reported in previous studies. Instead, it was related to the plate yield strength and plate thickness. The maximum tensile residual stress ratio decreases with an increase in both the yield strength and plate thickness.
- (3) The average magnitude of the compressive residual stress ratio over the middle part of the component steel plates was strongly influenced by the width-to-thickness ratio and plate yield strength, and closely related to the plate thickness. It should be noted that the average compressive residual stress ratio decreases with the increase in both the plate width-to-thickness ratio and yield strength.
- (4) Previous distribution models for the NSS and HSS welded box sections cannot be employed for HNHSS welded box sections. An improved residual stress model and the corresponding simplified prediction equations were established for predicting the residual stress of the welded box

sections that are fabricated by steel plates with yield strength varying from 300-MPa to 700-MPa. In such welded box sections, the steel yield strength and thickness of the flange plate may be different from those of the web plate. The effects of the plate yield strength, width-to-thickness ratio of plate, and the thickness of plate were taken into consideration in the proposal residual stress model.

Future experimental studies of HNHSS welded sections will be undertaken by the authors. As a preliminary exploratory study, the distribution and magnitude of residual stresses for NSS, HSS and HNHSS sections are compared in this paper. The experimental data and conclusions are helpful to applying HNHSS sections in steel structures.

## Acknowledgments

This research was financially supported by the National Key Research and Development Program of China (2017YFC0703400), the National Natural Science Foundation of China (51508205), the Guangdong Province Special Support Program “Innovating Science and Technology for Young Top Talents” (2016TQ03Z528), and the Fundamental Research Funds for the Central Universities (D2191360). The third author was supported through a postdoctoral fellowship provided by an Australian Research Council (ARC) Linkage Project (LP 150101196) awarded to the fourth author. All the sources of support are gratefully acknowledged.

## References

- An, G., Woo, W. and Park, J. (2019), “Welding residual stress effect in fracture toughness”, *J. Nanosci. Nanotech.*, **19**(4), 2323-2328. <https://doi.org/10.1166/jnn.2019.16008>
- ANSI/AISC360-10 (2010), Specification for Structural Steel Buildings; American Institute of Steel Construction, Chicago, IL, USA.
- Ban, H.Y., Shi, G., Shi, Y.J. and Wang, Y.Q. (2013), “Residual stress of 460 MPa high strength steel welded box section: Experimental investigation and modeling”, *Thin-Wall. Struct.*, **64**, 73-82. <https://doi.org/10.1016/j.tws.2012.12.007>
- Besovic, M. (2012), “Experimental investigation of residual stresses in cold formed steel sections”, *Steel Compos. Struct., Int. J.*, **12**(6), 465-489. <https://doi.org/10.12989/scs.2012.12.6.465>
- Cai, Y. and Young, B. (2019), “Experimental investigation of carbon steel and stainless steel bolted connections at different strain rates”, *Steel Compos. Struct., Int. J.*, **30**(6), 551-565. <https://doi.org/10.12989/scs.2019.30.6.551>
- Cao, X., Xu, Y., Wang, M., Zhao, G., Gu, L. and Kong, Z. (2018), “Experimental study on the residual stresses of 800 MPa high strength steel welded box sections”, *J. Constr. Steel Res.*, **148**, 720-727. <https://doi.org/10.1016/j.jcsr.2018.06.019>
- Chen, X. and Shi, G. (2019), “Cyclic tests on high strength steel flange-plate beam-to-column joints”, *Eng. Struct.*, **186**, 564-581. <https://doi.org/10.1016/j.engstruct.2019.01.093>
- Chen, Z., Liu, X. and Zhou, W. (2018), “Residual bond behavior of high strength concrete-filled square steel tube after elevated temperatures”, *Steel Compos. Struct., Int. J.*, **27**(4), 509-523. <https://doi.org/10.12989/scs.2018.27.4.509>
- Choi, J.Y. and Kwon, Y.B. (2018), “Direct strength method for high strength steel welded section columns”, *Steel Compos. Struct., Int. J.*, **29**(4), 509-526. <https://doi.org/10.12989/scs.2018.29.4.509>
- Estuar, F. and Tall, L. (1963), “Experimental investigation of welded built-up columns”, *Welding J.*, **42**, 164-s-176-s.
- Eurocode 3 (2005), Design of Steel Structures—Part 1-1: General Rules and Rules for Buildings; European Committee for Standardization, Brussels, Belgium.
- European Convention for Constructional Steelworks (ECCS) (1976), Manual on stability of steel structures: Part 2.2. Mechanical properties and residual stresses; ECCS Publ., Bruxelles, Belgium.
- Fang, H., Chan, T.-M. and Young, B. (2018), “Structural performance of cold-formed high strength steel tubular columns”, *Eng. Struct.*, **177**, 473-488. <https://doi.org/10.1016/j.engstruct.2018.09.082>
- Farahi, M. and Erfani, S. (2017), “Employing a fiber-based finite-length plastic hinge model for representing the cyclic and seismic behaviour of hollow steel columns”, *Steel Compos. Struct., Int. J.*, **23**(5), 501-516. <https://doi.org/10.12989/scs.2017.23.5.501>
- Feng, L. and Qian, X. (2018), “Low cycle fatigue test and enhanced lifetime estimation of high-strength steel S550 under different strain ratios”, *Marine Struct.*, **61**, 343-360. <https://doi.org/10.1016/j.marstruc.2018.06.011>
- Gardner, L., Bu, Y. and Theofanous, M. (2016), “Laser-welded stainless steel I-sections: Residual stress measurements and column buckling tests”, *Eng. Struct.*, **127**, 536-548. <https://doi.org/10.1016/j.engstruct.2016.08.057>
- GB50017-2017 (2017), Code for design of steel structures; China Planning Press, Beijing, China.
- Gou, R., Yu, M., Zhang, Y. and Xu, X. (2014), “Residual stress measurement of 1500 m(3) spherical tanks by X-ray diffraction method”, *Insight*, **56**(1), 26-30. <https://doi.org/10.1784/insi.2014.56.1.26>
- Hwang, I.-H., Chun, H.-J., Hong, I.-P., Park, Y.-B. and Kim, Y.-J. (2015), “Change of transmission characteristics of FSSs in hybrid composites due to residual stresses”, *Steel Compos. Struct., Int. J.*, **19**(6), 1501-1510. <https://doi.org/10.12989/scs.2015.19.6.1501>
- Javidan, F., Heidarpour, A., Zhao, X.L. and Minkinen, J. (2016), “Application of high strength and ultra-high strength steel tubes in long hybrid compressive members: Experimental and numerical investigation”, *Thin-Wall. Struct.*, **102**, 273-285. <https://doi.org/10.1016/j.tws.2016.02.002>
- Javidan, F., Heidarpour, A., Zhao, X.-L. and Al-Mahaidi, R. (2018), “Structural coupling mechanism of high strength steel and mild steel under multiaxial cyclic loading”, *Steel Compos. Struct., Int. J.*, **27**(2), 229-242. <https://doi.org/10.12989/scs.2018.27.2.229>
- Jiang, J., Lee, C.K. and Chiew, S.P. (2015), “Residual stress and stress concentration effect of high strength steel built-up box T-joints”, *J. Constr. Steel Res.*, **105**, 164-173. <https://doi.org/10.1016/j.jcsr.2014.11.008>
- Kang, L., Ge, H.B., Suzuki, M. and Wu, B. (2018a), “An average weight whole-process method for predicting mechanical and ductile fracture performances of HSS Q690 after a fire”, *Constr. Build. Mater.*, **191**, 1023-1041. <https://doi.org/10.1016/j.conbuildmat.2018.10.068>
- Kang, L., Suzuki, M., Ge, H.B. and Wu, B. (2018b), “Experiment of ductile fracture performances of HSS Q690 after a fire”, *J. Constr. Steel Res.*, **146**, 109-121. <https://doi.org/10.1016/j.jcsr.2018.03.010>
- Khan, M., Paradowska, A., Uy, B., Mashiri, F. and Tao, Z. (2016), “Residual stresses in high strength steel welded box sections”, *J.*



- Constr. Steel Res.*, **116**, 55-64.  
<https://doi.org/10.1016/j.jcsr.2015.08.033>
- Klotz, U.E., Zraggen, M., Von Trzebiatowski, O., Schindler, H.J., Winkler, M. and Pitschieler, K. (2002), "Residual stress measurement on a welded box beam section", *Materialwissenschaft Und Werkstofftechnik*, **33**(9), 544-549.  
[https://doi.org/10.1002/1521-4052\(200209\)33:9<544::AID-MAWE544>3.0.CO;2-4](https://doi.org/10.1002/1521-4052(200209)33:9<544::AID-MAWE544>3.0.CO;2-4)
- Li, T.-J., Li, G.-Q. and Wang, Y.-B. (2015), "Residual stress tests of welded Q690 high-strength steel box- and H-sections", *J. Constr. Steel Res.*, **115**, 283-289.  
<https://doi.org/10.1016/j.jcsr.2015.08.040>
- Lian, M., Su, M.Z. and Guo, Y. (2015), "Seismic performance of eccentrically braced frames with high strength steel combination", *Steel Compos. Struct., Int. J.*, **18**(6), 1517-U217.  
<https://doi.org/10.12989/scs.2015.18.6.1517>
- Nagaraja Rao, N. and Tall, L. (1961), "Residual stresses in welded plates", *Welding J.*, **40**(10), 468-s-105-s.
- Nie, S., Zhu, Q., Yang, B. and Li, P. (2018), "Investigation of residual stresses in Q460GJ steel plates from medium-walled box sections", *J. Constr. Steel Res.*, **148**, 728-740.  
<https://doi.org/10.1016/j.jcsr.2018.06.028>
- Qiang, X.H., Jiang, X., Bijlaard, F.S.K. and Kolstein, H. (2016), "Mechanical properties and design recommendations of very high strength steel S960 in fire", *Eng. Struct.*, **112**, 60-70.  
<https://doi.org/10.1016/j.engstruct.2016.01.008>
- Rasmussen, K.J.R. and Hancock, G.J. (1988), "Deformations and residual stresses induced in channel section columns by presetting and welding", *J. Constr. Steel Res.*, **11**(3), 175-204.  
[https://doi.org/10.1016/0143-974X\(88\)90041-7](https://doi.org/10.1016/0143-974X(88)90041-7)
- Saliba, N.G., Tawk, I. and Gergess, A.N. (2018), "Finite element modeling of rolled steel shapes subjected to weak axis bending", *Steel Compos. Struct., Int. J.*, **29**(2), 161-173.  
<https://doi.org/10.12989/scs.2018.29.2.161>
- Somodi, B. and Kovesdi, B. (2017), "Residual stress measurements on cold-formed HSS hollow section columns", *J. Constr. Steel Res.*, **128**, 706-720.  
<https://doi.org/10.1016/j.jcsr.2016.10.008>
- Somodi, B. and Koevesdi, B. (2018), "Residual stress measurements on welded square box sections using steel grades of S235-S960", *Thin-Wall. Struct.*, **123**, 142-154.  
<https://doi.org/10.1016/j.tws.2017.11.028>
- Taheri-Behrooz, F., Aliha, M.R.M., Maroofi, M. and Hadizadeh, V. (2018), "Residual stresses measurement in the butt joint welded metals using FSW and TIG methods", *Steel Compos. Struct., Int. J.*, **28**(6), 759-766. <https://doi.org/10.12989/scs.2018.28.6.759>
- Tebedge, N., Alpsten, G. and Tall, L. (1973), "Residual-stress measurement by the sectioning method", *Experim. Mech.*, **13**(2), 88-96. <https://doi.org/10.1007/BF02322389>
- Wang, Y.-B., Li, G.-Q. and Chen, S.-W. (2012), "The assessment of residual stresses in welded high strength steel box sections", *Journal of Constructional Steel Research*, **76**, 93-99.  
<https://doi.org/10.1016/j.jcsr.2012.03.025>
- Wang, W.Y., Qin, S.Q., Kodur, V. and Wang, Y.H. (2018), "Experimental study on evolution of residual stress in welded box-sections after high temperature exposure", *Adv. Steel Constr.*, **14**(1), 73-89.  
<https://doi.org/10.18057/IJASC.2018.14.1.5>
- Wang, Z., Deng, L. and Zhao, J. (2019), "A novel method to extract the equi-biaxial residual stress and mechanical properties of metal materials by continuous spherical indentation test", *Mater. Res. Express*, **6**(3), 036512.  
<https://doi.org/10.1088/2053-1591/aaeca6>
- Yuan, H.X., Wang, Y.Q., Shi, Y.J. and Gardner, L. (2014), "Residual stress distributions in welded stainless steel sections", *Thin-Wall. Struct.*, **79**, 38-51.  
<https://doi.org/10.1016/j.tws.2014.01.022>
- Zhang, X., Liu, S., Zhao, M. and Chiew, S.-P. (2016), "Residual stress of cold-formed thick-walled steel rectangular hollow sections", *Steel Compos. Struct., Int. J.*, **22**(4), 837-853.  
<https://doi.org/10.12989/scs.2016.22.4.837>
- Zhang, X., Huang, Z., Chen, B., Zhang, Y., Tong, J., Fang, G. and Duan, S. (2019), "Investigation on residual stress distribution in thin plate subjected to two sided laser shock processing", *Optics Laser Technol.*, **111**, 146-155.  
<https://doi.org/10.1016/j.optlastec.2018.09.035>

DL